

**FABRICATION OF COLLOIDAL PHOTONIC  
CRYSTALS VIA LANGMUIR BLODGETT  
TECHNIQUE AND THEIR INTEGRATION OF  
POLYMER MATRIX**

**A Thesis Submitted to  
the Graduate School of Engineering and Sciences of  
İzmir Institute of Technology  
in Partial Fulfillment of the Requirements for the Degree of**

**MASTER OF SCIENCE**

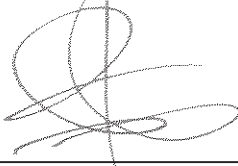
**in Materials Science and Engineering**

**by  
Ezgi İNCİ**

**July 2019  
İZMİR**

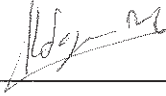
We approve the thesis of Ezgi İNCİ

**Examining Committee Members:**



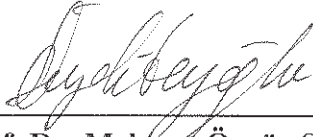
**Prof. Dr. Mustafa M. DEMİR**

Department of Materials Science and Engineering, İzmir Institute of Technology



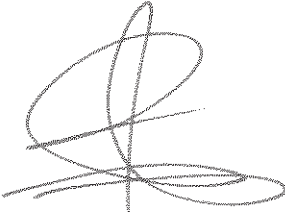
**Assoc. Prof. Dr. Yaşar AKDOĞAN**

Department of Materials Science and Engineering, İzmir Institute of Technology



**Prof. Dr. Mehmet Özgür SEYDİBEYOĞLU**

Department of Materials Science and Engineering, İzmir Katip Çelebi University



**Prof. Dr. Mustafa M. DEMİR**

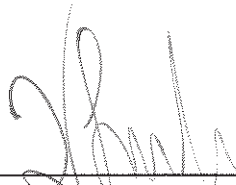
Supervisor, Department of Materials  
Science and Engineering,  
İzmir Institute of Technology

4 July 2019



**Prof. Dr. Canan VARLIKLI**

Co-Supervisor, Department of  
Photonics,  
İzmir Institute of Technology



**Assoc. Prof. Dr. Haldun SEVİNÇLİ**

Head of the Department of Materials  
Science and Engineering

**Prof. Dr. Aysun SOFUOĞLU**

Dean of Graduate School of  
Engineering and Science

## ACKNOWLEDGMENTS

Firstly, I would like to express my deepest gratitude to my advisor, Prof. Mustafa M. DEMİR, for his excellent guidance, caring, patience, confidence, friendship and providing me throughout this journey.

I would like to thank to my co-advisor Prof. Dr. Canan VARLIKLI with her suggestions and helping to this thesis. Also, I would like to thank to members of the thesis committee,

Prof. Dr. Mehmet Özgür SEYDİBEYOĞLU, Assoc. Prof. Dr. Yaşar AKDOĞAN and also Prof. Dr. Mustafa M. DEMİR for their valuable comments and suggestions.

I thank to Gökhan TOPÇU for his support and collaboration. I want to also thank to the members of Demir Research Group including Tuğba IŞIK, Tuğrul GÜNER, Hürriyet YÜCE, Tuğçe Aybüke Arıca GÜVENÇ, Çetin Meriç GÜVENÇ, Emre KARABURUN, Mehmet BAŞKURT, Mehmet ÖZCAN, Anılcan KUŞ, Rabia ÖNEN, and Mehmet Yenal YALÇINKAYA for their friendship and support. A special thanks to faculty members of Materials Science and Engineering. Also, I would like to thank to Polat BULANIK for his technical support.

I would like to thank my lovely fiancé for his support all during my MSc and my all life. He has constantly supported and encouraged me to follow my dreams and never give up.

I wish to thank all of my family and friends for their supports. I dedicate this thesis to my lovely family.

This thesis is supported by Scientific and Technological Research Council of Turkey (TÜBİTAK-117Z331).

## ABSTRACT

### FABRICATION OF COLLOIDAL PHOTONIC CRYSTALS VIA LANGMUIR BLODGETT TECHNIQUE AND THEIR INTEGRATION OF POLYMER MATRIX

Colloidal films have potential uses in various fields such as photonics, electronics, sensors, membrane filters, and surface devices owing to their unique optical properties. Photonic crystals composed of uniform diameter colloidal silica particles have been arranged in a periodic structure by taking inspiration from nature. The periodic structure of silica particles has physical interaction with light in a visible range. This special interaction is known as structural coloration. The close-packed monolayers and multilayers of colloidal silica particles in large area can be produced by using Langmuir Blodgett method. The integration of these photonic films with transparent polymer matrices having an elastomer feature provides for their use in optical sensor applications. In this thesis, we examined the fabrication of mechano-sensitive nanostructured films based on colloidal particles. Silica colloidal particles were synthesized at different sizes by using Stöber Process. Langmuir-Blodgett deposition was used to create three-layer of photonic crystal films with different particle diameters. For this purpose, various substrates were examined for the Langmuir Blodgett deposition process before starting the coating. The coated silica particles on the glass substrate were then embedded in an elastomeric transparent matrix. The generation of structural coloration after stretching was examined in manufactured elastomer films. In accordance with this purpose, various polymers such as acrylates and siloxanes with elastomer properties have been used. The structural characterization of these composite films and their optical properties were summarized in this thesis.

# ÖZET

## KOLLOİDAL FOTONİK KRİSTALLERİN LANGMUIR BLODGETT TEKNİĞİ İLE ÜRETİLMESİ VE POLİMER MATRİSİNE ENTEGRASYONU

Kolloidal filmler, benzersiz optik özelliklerinden dolayı fotonik, elektronik, sensörler, membran filtreler ve yüzey cihazları gibi potansiyel uygulama alanlarına sahiptirler. Özdeş boyutlara sahip kolloidal silika parçacıklarından oluşan fotonik kristaller, doğadan ilham alınarak periyodik bir yapıda düzenlenmişlerdir. Silika parçacıklarının periyodik yapısı, görünür bölgede ışıkla fiziksel bir etkileşime sahiptir. Bu özel etkileşim yapısal renklendirme olarak bilinir. Langmuir Blodgett yöntemi kullanılarak büyük ölçüde sıkı paketlenmiş tek katmanlı ve çok katmanlı kolloidal silika parçacıkları üretilebilir. Bu fotonik filmlerin elastomer özelliğe sahip polimer matrisler ile entegrasyonları, optik sensör uygulamalarında kullanılmalarını sağlar. Bu tezde, kolloidal nanoparçacıklara dayalı, mekanik etkiye duyarlı nanoyapılı filmleri inceledik. Farklı boyutlara sahip silika parçacıkları Stöber prosesi kullanılarak sentezlendi. Farklı parçacık boyutlarına sahip üç katmanlı fotonik kristal filmleri oluşturmak için Langmuir Blodgett tekniği kullanıldı. Bu amaçla, kaplamaya başlamadan önce Langmuir Blodgett biriktirme işlemi için farklı alt taşlar incelendi. Daha sonra, cam alt taş üzerine kaplanan silika parçacıkları elastomerik şeffaf bir matris içerisine gömüldü. Germe sonrası yapısal renklenmenin oluşumu, üretilen elastomer filmlerde incelendi. Bu amaç doğrultusunda, elastomer özellikliğe sahip akrilatlar ve siloksanlar gibi çeşitli polimerik malzemeler denendiler. Bu kompozit filmlerin yapısal detayları ve optik özellikleri bu tezde özetlendi.

*Dedicated to my family...*

# TABLE OF CONTENTS

LIST OF FIGURES.....	ix
LIST OF TABLES.....	xii
LIST OF ABBREVIATIONS.....	xiii
CHAPTER 1. INTRODUCTION.....	1
1.1. Motivation.....	1
1.2. The Structure and Scope of the Thesis.....	2
1.3. State of Art: Langmuir Blodgett Deposition.....	3
CHAPTER 2. LITERATURE REVIEW.....	4
2.1. Structural Color.....	4
2.1.1. History of Structural Color.....	4
2.1.2. Basic Optical Mechanisms Related to Structural Colors.....	5
2.2. Photonic Crystals.....	7
2.2.1. Derivation of Bragg-Snell Law for Opal Structures.....	9
2.3. Colloid Based on Materials.....	10
2.4. Langmuir Blodgett Deposition.....	12
2.4.1. History of Langmuir Blodgett Film.....	12
2.4.2. Working Principle of Langmuir Blodgett Deposition.....	12
2.4.3. Surface Tension and Surface Pressure.....	12
2.4.4. Monolayers of Water-Soluble Materials.....	13
2.4.5. Surface Pressure and Area Isotherms.....	13
2.5. Colloidal Silica Nanoparticles.....	14
2.5.1. Synthesis of Silica Particles Using Stöber Process.....	14
CHAPTER 3. EXPERIMENTAL.....	16
3.1. Materials.....	16

3.2. Methods .....	16
3.2.1. Synthesis of Silica Particles .....	16
3.2.2. Surface Modification of SiO <sub>2</sub> Particles.....	17
3.2.3. Preparation of Glass Substrates .....	17
3.2.4. Preparation of the Langmuir-Blodgett Films.....	17
3.2.5. Synthesis of Poly (Ethyl Acrylate-Co-Methyl Methacrylate) By Free Radical Polymerization.....	18
3.2.6. Fabrication of Elastomer SiO <sub>2</sub> /PDMS Film.....	19
3.2.7. Fabrication of Strain Responsive Elastomer SiO <sub>2</sub> /P(PEGPEA) Films.....	19
3.3. Characterization .....	20
CHAPTER 4. RESULTS AND DISCUSSION.....	21
4.1. Synthesis of SiO <sub>2</sub> Colloids.....	21
4.2. Investigation of Various Substrates .....	22
4.3. Langmuir Blodgett Films and Their Elastomeric Matrix Composite .....	26
4.4. Monomer/Silica Monolayers Produced from Different Vinyl Monomers. ....	27
4.5. Polymer/Silica Monolayers.....	29
4.6. PDMS/SiO <sub>2</sub> Elastomer Composite .....	31
4.7. Elastomer P(PEGPEA)/Silica Photonic Crystal .....	33
4.7.1. Three-Layers Photonic Crystals.....	33
4.7.2. Morphological Properties of Three-Layers LB Films .....	35
4.7.3. Optical Properties of Three-Layers LB Films .....	37
4.7.4. Elastomer P(PEGPEA)/Silica Composite.....	40
CHAPTER 5. CONCLUSIONS .....	46
REFERENCES .....	47



# LIST OF FIGURES

<u>Figure</u>	<u>Page</u>
Figure 1.1. Photographs of Langmuir Blodgett device (a) all components of device (b) important Langmuir trough components to obtain monolayer on the water sub-phase.....	3
Figure 2.1. (a) Morpho menelaus butterfly photograph. Inset, the butterfly's wing is wetted with ethanol (Source: Mason, C. W, 1926) <sup>24, 25</sup> , (b) photograph of peacock feather. Inset, the eye region of an adult peacock feather (Source: Mason, C. W, 1927). <sup>25</sup> .....	5
Figure 2.2. SEM images of the Morpho butterfly wing: (a) low magnification image; (b) high magnification image; (c) ground scale image; (d) cover scale image (Source: Jiang and McFarland, 2004). <sup>9</sup> .....	6
Figure 2.3. Schematic illustration of the 1D, 2D, 3D of photonic crystals (Source: Joannopoulos et al. 2008). <sup>31</sup> .....	7
Figure 2.4. Illustration of the interaction of light with a periodic material (Source: Armstrong and O'Dwyer, 2015). <sup>32</sup> .....	8
Figure 2.5. Schematic illustration of the diffraction from opal silica matrix (Source: Tilley, 2010). <sup>34</sup> .....	9
Figure 2.6. Photographs of the stretched colloidal crystal elastomer (a), and its UV–vis absorption spectra (b) (Source: Ito et al. , 2013). <sup>42</sup> .....	11
Figure 2.7. (a) Pressure-area isotherm for a monolayer of stearic acid on ultrapure water. (b) molecular configuration in the three regions gaseous phase, liquid-expanded phase, and condensed phase, respectively (Source: Oliveira, 1992). <sup>45</sup> .....	14
Figure 2.8. Synthesis of silica particles via Stöber process. ....	15
Figure 3.1. Schematic representation of fabrication of the three-layer LB films. ....	18
Figure 3.2. Schematic representation of the fabrication of PDMS/ SiO <sub>2</sub> film.....	19
Figure 3.3. Schematic representation of photopolymerization process. ....	20
Figure 4.1. DLS size distribution of SiO <sub>2</sub> particles.....	21

<b><u>Figure</u></b>	<b><u>Page</u></b>
Figure 4.2. Isotherm curves for various substrates. ....	23
Figure 4.3. SEM images of SiO <sub>2</sub> particles coated with Langmuir Blodgett method on various substrates .....	24
Figure 4.4. Photographs of various substrates coated with three-layers of SiO <sub>2</sub> .....	24
Figure 4.5. Reflection spectra of three-layer SiO <sub>2</sub> particles with various substrates.....	25
Figure 4.6. Isotherm curves of different monomer/ SiO <sub>2</sub> dispersions. ....	27
Figure 4.7. Isotherm curve of polymer/ SiO <sub>2</sub> dispersion.....	29
Figure 4.8. Photograph of P (EA-co-MMA)/ SiO <sub>2</sub> dispersion (a) during LB coating, (b) LB coated image, (c) P (EA-co MMA) film casting on film. ....	30
Figure 4.9. (a) SEM image of the thick layer polymer /SiO <sub>2</sub> coating, (b) AFM image of the polymer/silica coating deposited with LB method. ....	31
Figure 4.10. SEM images of three-layers SiO <sub>2</sub> particles produced by the Langmuir Blodgett method. ....	31
Figure 4.11. SEM images of SiO <sub>2</sub> / PDMS elastomer (Inset: FFT image of polymer film).....	32
Figure 4.12. Transmittance spectrum of SiO <sub>2</sub> /PDMS composite before and after strain.....	33
Figure 4.13. Isotherm curves of three-layers SiO <sub>2</sub> particles.....	34
Figure 4.14. SEM images of three-layers SiO <sub>2</sub> particles produced by LB method (Inset: corresponding FFT images). ....	35
Figure 4.15. (a) Calculated radial distribution functions of colloidal arrays and (b) its schematic representation.....	36
Figure 4.16. AFM image of three-layers photonic crystal, (a) 2D and (b) 3D image.....	37
Figure 4.17. Reflection spectra of photonic crystal films with various diameter, (a) 175 nm, (b) 230 nm, (c) 280 nm respectively.....	38
Figure 4.18. Photographs of three-layers SiO <sub>2</sub> films with various diameter. ....	39
Figure 4.19. Photographs of three-layers SiO <sub>2</sub> films with various angle.....	40
Figure 4.20. SEM images of P(PEGPEA)/ SiO <sub>2</sub> composite film.....	41
Figure 4.21. SEM cross section images of 230 nm composite film.....	42

<b><u>Figure</u></b>	<b><u>Page</u></b>
Figure 4.22. Photographs of P(PEGPEA)/SiO <sub>2</sub> composite film with various angles. ....	42
Figure 4.23. Normalized reflection spectra of P(PEGPEA)/SiO <sub>2</sub> composite film. ....	43
Figure 4.24. Reflection spectra of the P(PEGPEA)/silica composite film upon lateral strain. ....	43
Figure 4.25. Schematic representation of structure of the strain responsive elastomer. ....	44
Figure 4.26. Change in (a) reflection signal, (b) thickness, and d (111) as a function of applied strain. ....	44
Figure 4.27. Reversible optical properties of the films; (a) alter in reflection upon gradual stretching-releasing. (b) The reflection signals as a function of cycles between lateral strains of 0-40%. ....	45

# LIST OF TABLES

<u>Table</u>	<u>Page</u>
Table 2.1. Types of colloid based on materials, their applications, and advantages.....	10
Table 4.1. Detailed information about to resulting colloidal SiO <sub>2</sub> particles; conditions of reaction, size, and zeta potential.....	22
Table 4.2. Parameters of monomer/SiO <sub>2</sub> coating and results .....	28

## LIST OF ABBREVIATIONS

AFM	Atomic Force Microscopy
CBM	Colloid Based Materials
DLS	Dynamic Light Scattering
D	Interplanar distance
fcc	Face centered cubic
hcp	Hexagonal close-packed
LB	Langmuir Blodgett
m	Order of diffraction
$n_s$	Refractive index of the opal matrix
PDMS	Polydimethylsiloxane
P(PEGPEA)	Poly (ethylene glycol) phenyl ether acrylate
SEM	Scanning Electron Microscopy

# CHAPTER 1

## INTRODUCTION

### 1.1. Motivation

An enormous number of orders and patterns have been created spontaneously in the natural world. Structural color is one of the most impressive consequences of such processes. In general, there are two ways to create color. In the first one, color arises from the absorption of light in the ordinary coloring mechanism. Pigments, dyes and metals have such an absorption mechanism. In this case, the color is produced by the changing of energies between light and electron in the matter. In the second case, the coloration is a physical procedure of light interacting with the materials. This mechanism is called structural coloration. Structural color in nature originates from thin-film interference, multilayer interference, diffraction grating, light scattering, and photonic crystal.<sup>1</sup>

Structural color iridescence means that color changes depending on the viewing angle. Moreover, photonic crystals perform the Bragg-Snell law, and then the color is generated with the diversified angle of the incident light. Opal gemstones,<sup>2</sup> beetles,<sup>3</sup> bird feathers,<sup>4</sup> and butterfly wings<sup>5</sup> are commonly found photonic crystals in nature. Many organisms can adjust their structural colors for camouflage, warning enemies or communicating in response to the surrounding environment.<sup>6</sup> Inspired by nature, PCs have been created for the application of colorimetric sensors. The sensors are produced with materials which react to external stimuli.<sup>7</sup>

Periodic crystals have been fabricated artificially by colloidal photonic crystals capable of reflecting light on a precise photonic stop band. Multiple scalable methods such as self-assembly,<sup>8</sup> spin coating,<sup>9</sup> spray process,<sup>10</sup> electrophoresis,<sup>11</sup> solvent evaporation,<sup>12, 13</sup> and deposition of Langmuir-Blodgett (LB) have been studied in this state to create colloidal three-dimensional networks. For example, Topçu et. al., produced uniform sized SiO<sub>2</sub> colloids by using a solvent evaporation method.<sup>13</sup> Similarly, through

spraying polymeric colloids, Zeng et al.<sup>10</sup> produced non-iridescent structural colored fabrics. The assembly of colloidal particles into photonic crystals using the LB technique has been reported in numerous papers. This layer-by-layer photonic crystal manufacturing enables both monolayer and multilayer films to be controlled.

Photonic structures with colloidal arrays and elastic matrix enable stimuli-responsive materials to be created. For instance, the use of gel matrices is the strategy that has been widely examined because the colloidal particle self-assembly in a liquid state is more appropriate. Core-shell melt extrusion is being used to produce elastomeric, mechanically robust opals over large regions.<sup>14</sup> Dengteng Ge and coworkers have reported a smart robust window that displays angle-independent reflective colors. They have used PDMS as an elastomer matrix.<sup>15</sup> The mechanochromic photonic film was produced by using colloidal SiO<sub>2</sub> particles, which were embedded in an elastomer matrix. In this thesis, P(PEGPEA) was used as the elastomer matrix and the photonic elastomer film was obtained by the photopolymerization method.

Langmuir–Blodgett technique allows the manufacture of highly ordered monomolecular films with exactly controlled thickness.<sup>16, 17</sup> Monolayers of hcp SiO<sub>2</sub> particle have been generated by using LB method and binary surfactant and solvent systems have been investigated. It was also reported that methanol used as a co-solvent improves interactions between particles and water, and increases particle hydrophobicity.

18

In this thesis, multilayer photonic films of colloidal SiO<sub>2</sub> particles were fabricated by using Langmuir-Blodgett deposition method that enables to controlled layer thickness and largely hexagonal close packed structure. Afterward, the integration of the resulting films into the various polymer matrix have been investigated. In this context, the resulting polymer composite films maintain its structural color as photonic crystal films consisting only colloidal SiO<sub>2</sub> particles. Moreover, the generation of structural coloration upon stretching was examined in fabricated elastomer films.

## **1.2. The Structure and Scope of the Thesis**

The first chapter presents the thesis introduction. A comprehensive review of the literature is done in Chapter 2. This section includes information on structural color, photonic crystals, methods of Langmuir Blodgett and colloidal SiO<sub>2</sub> particles. The

experimental part is given in Chapter 3, and the results of their discussions will be given in chapter 4. The final parts will be described in Chapter 5.

### 1.3. State of Art: Langmuir Blodgett Deposition

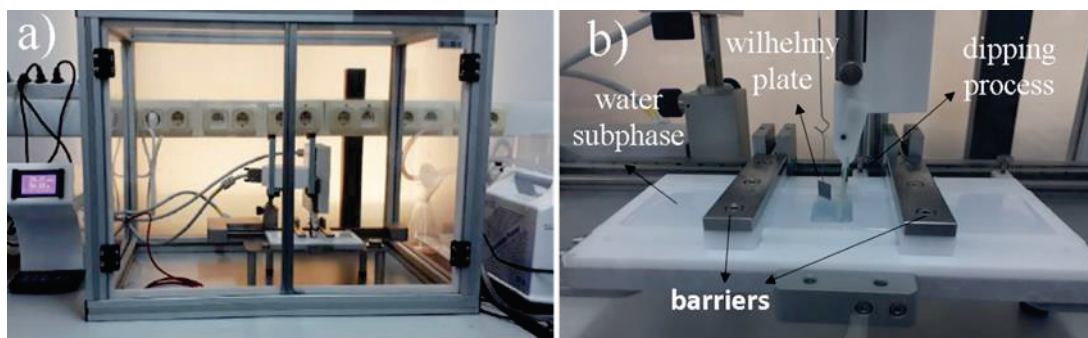


Figure 1.1. Photographs of Langmuir Blodgett device (a) all components of device (b) important Langmuir trough components to obtain monolayer on the water sub-phase

Typical Langmuir Blodgett (LB) devices include trough, barriers, Wilhelmy plate, dipping apparatus, and special software (Figure 1.1). The water sub-phase is placed in the hydrophobic LB trough and the amphiphilic material is spread over water sub-phase. Barriers provide compression to obtain ordered monolayer on the water surface. Wilhelmy plate measures the surface pressure and provides film balance with the software. The dipping process is very significant because it transfers the monolayer onto the solid substrates by moving the solid substrate up and down.

The technique of Langmuir-Blodgett is one of the most important methods for preparing thin films. This method enables:

- Precise monolayer thickness control,
- Homogeneous monolayer deposition over large areas,
- Multilayer thin films.



## CHAPTER 2

### LITERATURE REVIEW

#### 2.1. Structural Color

Pigments, structural colors, and bioluminescence are the main sources of coloring in nature. The most interesting one is structural coloration due to the interaction between the material's physical properties and the light.<sup>19</sup> Structural color derives from the diffraction of light owing to periodic micro or nanostructures of the materials.<sup>5</sup> In other words, structural coloration includes the partial reflection of incident light by a physical structure of materials.<sup>20</sup> Film interference, diffraction grating, scattering, and photonic crystals are primary structural color mechanisms.<sup>19</sup> An example of structural coloration in nature is brown-pigmented peacock tail feathers. Their organized structures reflect blue, turquoise and green colors (Figure 2.1.b). Another example is Morpho Menelaus butterfly wings, which are structurally blue due to their periodic microstructure on the wing (Figure 2.1.a). Structural colors have recently received attention as their usage has advanced rapidly in several areas such as textiles, automobiles, vision, cosmetics, and sensors.

##### 2.1.1. History of Structural Color

There is a long history in the study of structural colors. The *Micrographia*, written by Robert Hooke in 1665, was the oldest scientific work. This book described brilliant color properties of both peacock and duck feathers. He suggested that the light was strongly reflected by alternating layers of thin plates and air. Isaac Newton also described the color mechanism of the brown pigment of the peacock tail feathers via book *Optiks* in 1704. Iridescence of peacock feathers originally came from the thinness of the feather, according to his book. Thomas Young improved Newton's principle by showing that light

could also behave as a wave. He showed in 1803 that light can diffract from sharp edges, producing patterns with interference.<sup>21</sup> In 1917, Lord Rayleigh explored a formula for expressing the reflective properties of a periodically hierarchical environment utilizing electromagnetic theory and noted it to be the origin of the colors of certain crystals, probably of certain beets and butterflies.<sup>22</sup> Merritt evaluated the tempered steel and Morpho butterfly reflection spectrum. The author defined the outcomes as thin-layer interference.<sup>23</sup>

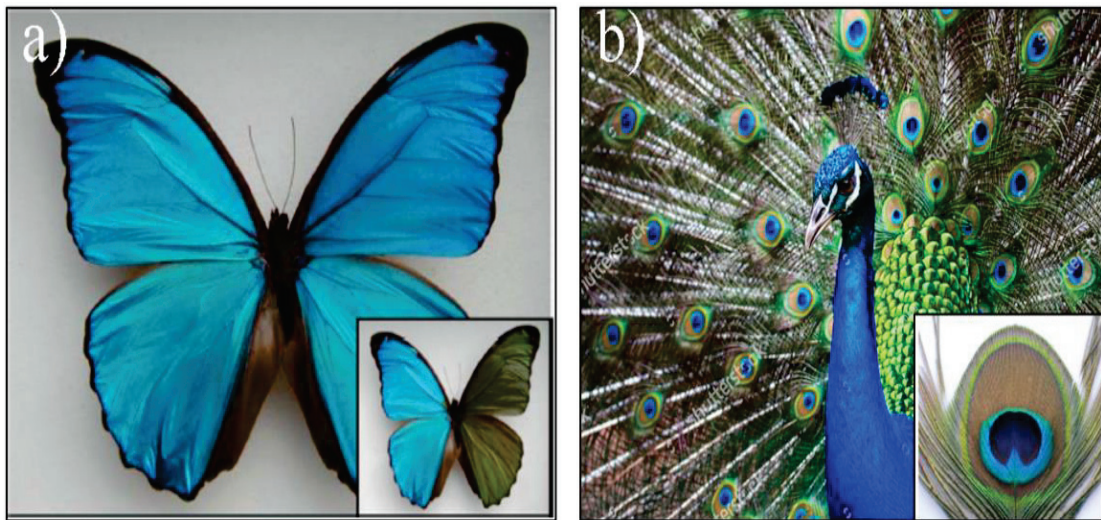


Figure 2.1. (a) Morpho menelaus butterfly photograph. Inset, the butterfly's wing is wetted with ethanol (Source: Mason, C. W, 1926)<sup>24, 25</sup>, (b) photograph of peacock feather. Inset, the eye region of an adult peacock feather (Source: Mason, C. W, 1927).<sup>25</sup>

### 2.1.2. Basic Optical Mechanisms Related to Structural Colors

Interference of the film in nature encompasses interference with both thin film and multilayer film. Thin film interference is observed in nature, where incoming light is reflected and interferes with the inner and outer boundaries.<sup>20</sup> Diffraction gratings are especially common in invertebrates. A diffraction grating made of layers of chitin and air gives rise to the iridescent colors of several butterfly wings, but also the tail feathers of birds such as the peacock. According to the perspective of physical mechanisms, both interference and diffraction can generate iridescent color, and also some forms of scattering create non-iridescent structural colors due to the irregularity of the structure.<sup>26</sup>

For iridescent blue color of Morpho butterfly, due to periodic microstructures, structural color generated owing to diffraction of the light.

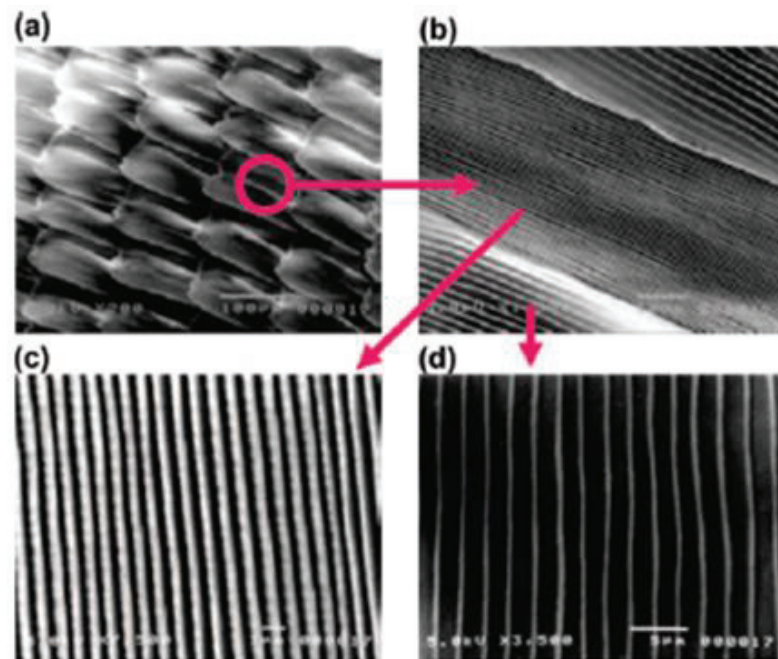


Figure 2.2. SEM images of the Morpho butterfly wing: (a) low magnification image; (b) high magnification image; (c) ground scale image; (d) cover scale image (Source: Jiang and McFarland, 2004).<sup>9</sup>

Figure 2.2 shows the SEM images of ordered Morpho Menelaus butterfly scales. On the wings of a butterfly, there are two different levels of length scales. These are called 'cover scales' and 'ground scales'. The butterfly's structural color produced by the ground scales. The ridges on the ground scales are aligned to each other in parallel. Furthermore, each ridge is structured by the existence of cuticles. They are ordered structure leads to the effects of interference. As a result, the interference effect and diffraction grating in the butterfly wings contribute to the blue color.<sup>27, 28</sup>

Light scattering is another origin of structural colors that differ from multilayer interference or photonic crystal as it arises in random structures. Lord Rayleigh described the source of the blue sky first as a consequence of light scattering by atmospheric particles. Mie scattering exists owing to increasing particle size, and the dependence on wavelength varies noticeably from Rayleigh scattering which means that several colors begins to appear. Because of the scattering of Mie, larger particles scatter red instead of blue in the Mars atmosphere. Scattering of light has often been described as a classic

example of non-iridescent structural colors in the literature. Mason noted that special insects colors were due to Tyndall blue, and a dragonfly's body, *Mesothemis simplicicollis*, and *Libellula pulchella*'s wing were evidenced.<sup>25</sup> Mason carried out investigations into many kinds of bird feathers and mentioned the similarities between their iridescent color.<sup>24</sup> Then electron microscopic studies in the feathers of peacocks, birds, and ducks discovered a surprisingly small structure. These animals formed a periodic submicron structure. Also, the periodicity of the structures is comparable to the visible light wavelength. The significance of optical interference was thought accordingly.<sup>29</sup> Photonic crystals are described as a medium with a refractive index which periodically varies in space.<sup>30</sup>

## 2.2. Photonic Crystals

Photonic crystals are composite media has produced periodically from materials with different dielectric constants and could be arranged in 1D, 2D or 3D.

Figure 2.3 shows that different colors represent various dielectric constants. Depending on the incident beam, the periodicity is related to the wavelength of visible light. Such a condition is defined by the Bragg-Snell Law.<sup>31</sup>

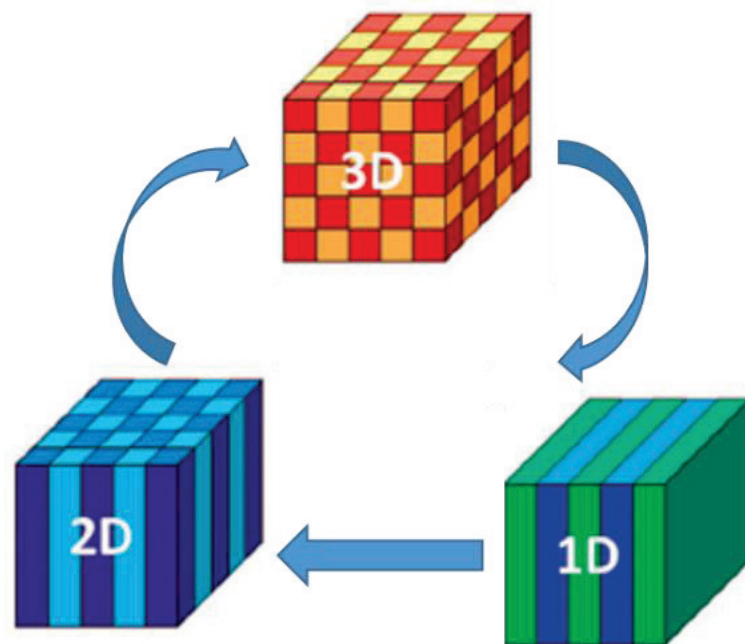


Figure 2.3. Schematic illustration of the 1D, 2D, 3D of photonic crystals (Source: Joannopoulos et al. 2008).<sup>31</sup>

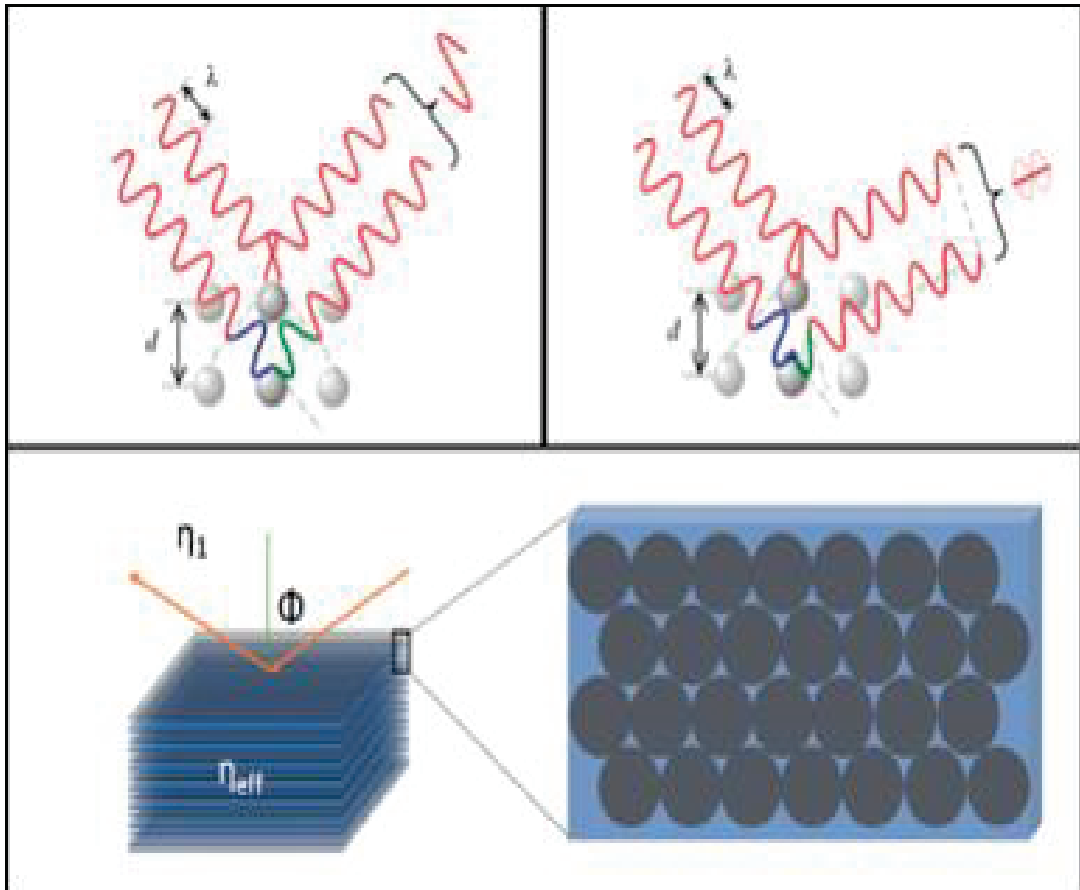


Figure 2.4. Illustration of the interaction of light with a periodic material (Source: Armstrong and O'Dwyer, 2015).<sup>32</sup>

Bragg-Snell law is derived from the combination of both Snell's law and Bragg's law. Figure 2.4 shows that the opal film has been designed as a two-medium multilayer with distinct refractive indices. From this case, indices ( $n_1$ ) is usually vacuum, air, or liquid, and the other ( $n_2$ ) is material. ( $n_{eff}$ ) is the media's effective refractive index. It depends on the spheres refractive indices and the refractive index of the environment.<sup>32</sup>

In response to external stimuli, several living organisms can reversibly alter their structural color. By taking inspiring such structures, photonic materials have been synthetically produced. In contrast, artificial photonic materials are less intelligent than natural structures. Due to diffraction falling into the visible range using photonic crystal, optical output was observed by naked eye. Colloid-based sensors can be restricted in a thin film or created as distinct super particles, which can be patterned spatially, chemically, and structurally, respectively. Therefore, they have been suitable for sensor applications. Vapor, solvent, temperature, ion, pH, and pressure are used as external stimuli for the application of colloidal photonic crystal for sensor applications.<sup>33</sup>

## 2.2.1. Derivation of the Bragg-Snell Law for Opal Structures

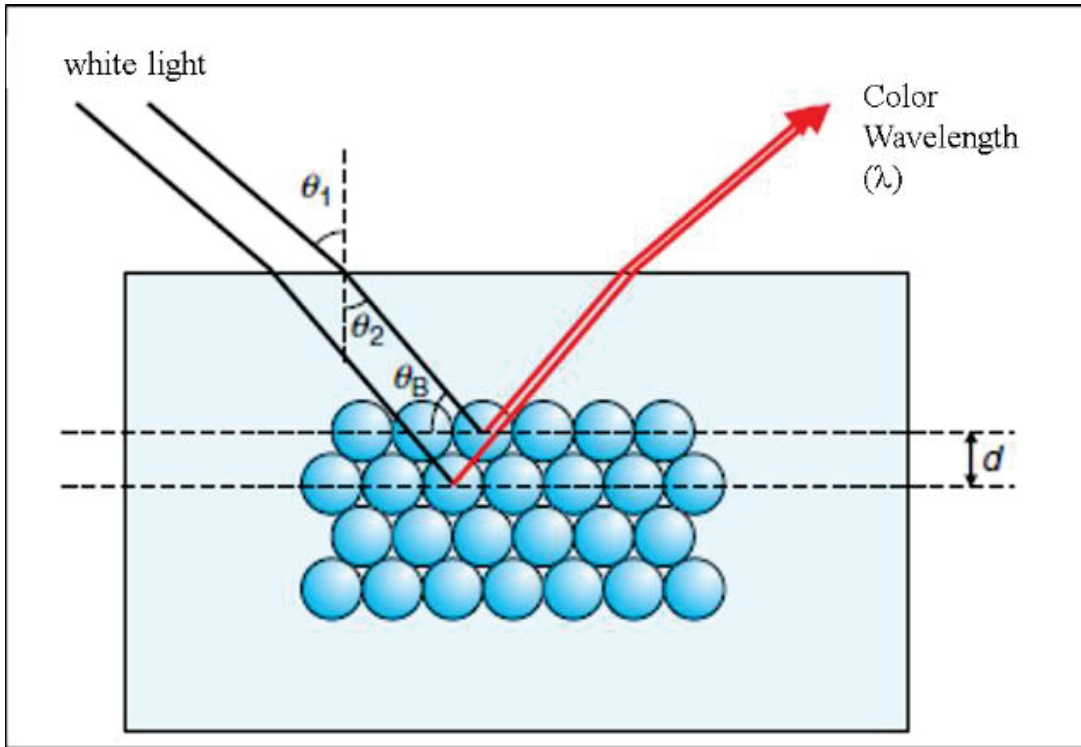


Figure 2.5. Schematic illustration of the diffraction from opal silica matrix (Source: Tilley, 2010).<sup>34</sup>

The color of the opal is caused by white light diffraction. Ordered packing of  $\text{SiO}_2$  spheres embedded in amorphous silica matrix in this case.  $\lambda_0$  is vacuum wavelength of the light and  $\theta_B$  is diffraction angle. The following equation provides a combination of Bragg and Snell law for opal.<sup>34</sup>

$$\lambda(\text{opal}) = \frac{\lambda_0}{n_s} \quad (1)$$

$$\theta_B = (90 - \theta_2) \quad (2)$$

From the Bragg equation;

$$m\lambda_0 = 2n_s d \sin \theta_B \quad (3)$$

$$m\lambda_0 = 2n_s d \sin(90 - \theta_2) \quad (4)$$

$$m\lambda_0 = 2n_s d \cos \theta_2 \quad (5)$$

$$m\lambda_0 = 2n_s d (1 - \sin^2 \theta_2)^{1/2} \quad (6)$$

Using Snell law;

$$\sin \theta_2 = \frac{\sin \theta_1}{n_s} \quad (7)$$

$$m\lambda = 2n_s d \left(1 - \frac{\sin^2 \theta_1}{n_s^2}\right)^{1/2} \quad (8)$$

$$= 2d(n_s^2 - \sin^2 \theta_1)^{1/2} \quad (9)$$

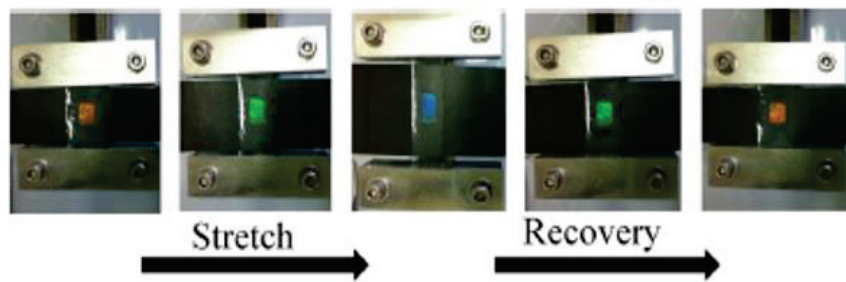
### 2.3. Colloidal Materials

Synthetically, monodisperse colloids can be produced. They used to develop structures commonly discovered in nature where simple building blocks are preferred to obtain a variety of functions despite a limited space of materials. Colloidal self-assembly creates nanoscale characteristics by using the bottom up methods. Taking the advantage of molecular interactions, the self-assembly provides simple, cost-effective and fast over large areas.<sup>35</sup> Colloids based materials range from 100 nm to 1000 nm.<sup>36</sup> The application areas of colloid based materials are optics,<sup>37</sup> wetting,<sup>38</sup> sensing,<sup>39</sup> catalysis,<sup>40</sup> and electrodes.<sup>41</sup>

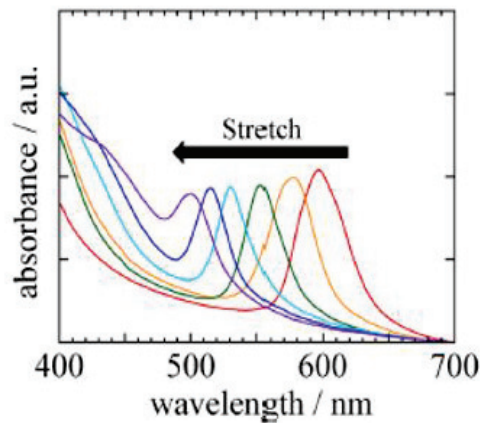
Table 2.1. Types of colloid based on materials, their applications, and advantages.

<u>Colloid Based Materials</u>	<u>Application Areas</u>	<u>Applications Benefit From</u>
Metal	Optics	The tunability
Metal oxide	Wetting	Tailorability
Polymer	Sensing	Hierarchy of CBM
	Catalysis	
	Electrodes	

Spherical colloidal particles are generally preferred by the self-assembly process to produce building blocks. Particularly, polystyrene, poly (methyl methacrylate), and silica are used as spherical particles. Colloids are effective in natural and biomimetic structural color applications because they have length scale which can be matched as the wavelength of the visible light. The conventional structures generated by spherical assemblies are opals in the periodic arrangement of the fcc crystal, composed of three-dimensional structures of colloidal particles.<sup>33</sup>



(a)



(b)

Figure 2.6. Photographs of the stretched colloidal crystal elastomer (a), and its UV–vis absorption spectra (b) (Source: Ito et al. , 2013).<sup>42</sup>

Tatsunori Ito and co-workers have defined elastomeric materials, which have tunable structural color upon stretching in their study. The reversible blue shift has been observed in elastomer due to Poisson ratio of the structure.<sup>42</sup> The film thickness shifts from red to blue depending on the stretching has been shown in Figure 2.6.(a). In addition to reversible color changing, the blue peak shift of stretching also has been shown in Figure 2.6.(b).



## **2.4. Langmuir Blodgett Deposition**

### **2.4.1. History of Langmuir Blodgett Film**

Agnes Pockels created the first suggestion to manipulate oil films on the surface of water in 1891, as she studied in her kitchen. Lord Rayleigh then presented the hierarchy on the water surface in 1899 for experiments with insoluble monolayers.<sup>43</sup> Additional experimental techniques enabled to calculate film thickness by Devaux.<sup>44</sup> Then, it's hard to find that without polar functional groups oils couldn't be spread across the water surface. Irving Langmuir investigated several new approaches for amphiphilic molecules at the air-water interface in 1917 and developed the Langmuir Blodgett trough. Moreover, Langmuir made a major contribution to literature in producing stable monolayer films. His assistant, Katherine Blodgett, carried out the return of fatty acid monolayers to a solid support. In 1935, Katherine Blodgett (1898-1979) investigated the transfer to floating monolayers onto the solid material as they were called to a substrate.

### **2.4.2. Working Principle of Langmuir Blodgett Deposition**

The material is dispersed in a proper volatile solvent (e.g. chloroform). Then, the dispersion spread onto an aqueous sub-phase surface. In a short period of time, the solvent evaporates, and the molecules spread over the entire water surface. The monolayer of the Langmuir is compressed till the molecules are regularly aligned. Langmuir Blodgett films are deposited by immersing a clean substrate in the aqueous sub-phase. Repeated dipping process produce multilayer structures.<sup>45</sup>

### **2.4.3. Surface Tension and Surface Pressure**

The surface pressure is the lowering of the liquid's surface tension with a monolayer on it. The relationship between surface pressure and surface tension is presented in the following equation;

$$\Pi = \gamma - \gamma_0 \quad (10)$$

$\gamma$  defines the surface tension when the monolayer is absent, and  $\gamma_0$  defines the surface tension at the existence of the monolayer. Wilhelmy plate provides to measure of

the surface pressure. Water has a surface tension value of 73 m/Nm. Explaining why water is most commonly used in the lower phase is the value of surface tension, which is much higher than that of other liquids.<sup>46</sup>

#### **2.4.4. Monolayers of Water-Soluble Materials**

Insoluble amphiphilic consisting of a polar head and a long non-polar chain are the most suitable materials for the use of Langmuir Blodgett method. Recently, however, highly periodic monolayers could be obtained at the air-water interface using lightly exchanged water soluble materials such as anionic or cationic surfactants. However, in this case, these water-soluble substances are required to interact with certain insoluble materials such as long-chain fatty acids or inert polymers in order to achieve a monolayer structure on the water sub-phase.<sup>47</sup>

Ordered monolayers and multilayers can be obtained due to the preference of amphiphilic materials. Also, the resulting films can be used for tunable physical, chemical and optical properties.<sup>48</sup>

#### **2.4.5. Surface Pressure and Area Isotherms**

When the surface area (' gas compression') is reduced, the density of molecules as well as the surface pressure increases. Previously, molecules are quite away from each other in the gaseous state and the distance between them is reduced depending on the compression process. As a result, the expanded liquid and condensed liquid states are respectively observed.<sup>49</sup> When the monolayer is spread in a large area, it can then be considered a monolayer as a two-dimensional gaseous. If a barrier system reduces the available surface area of the 2D monolayer, the molecules begin to impose a repulsive force on each other. Firstly, the monolayer is reached to the liquid phase. The liquid state is generally divided of liquid expanded and liquid condensed states.

Eventually, maintaining compression, molecules are very close to each other and becoming less compressible and 2D solid as a monolayer is produced (Figure 2.7, a-b). Then, transferring process is applied onto the ordered monolayered particles are deposited on the solid substrate. For condensed Langmuir films, surface pressure is usually higher than 15 mN/m and typically 30 mN/m.

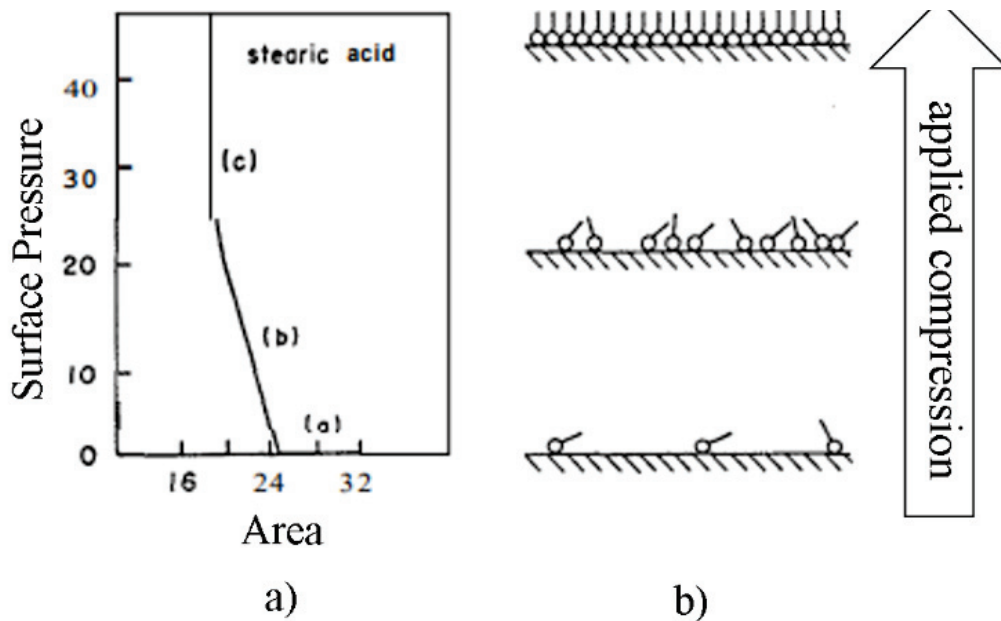


Figure 2.7. (a) Pressure-area isotherm for a monolayer of stearic acid on ultrapure water. (b) molecular configuration in the three regions gaseous phase, liquid-expanded phase, and condensed phase, respectively (Source: Oliveira, 1992).<sup>45</sup>

## 2.5. Colloidal Silica Nanoparticles

Silica is widely used across the world. Due to their controllable properties and composition, colloidal SiO<sub>2</sub> particles have recently drawn considerable attention in many various applications such as cosmetics, abrasive, food, drug, environmental care, dentistry, tissue engineering, etc. Surface chemistry, porosity, molecular structure and morphology affect the properties of colloidal SiO<sub>2</sub> particles. In literature, colloidal SiO<sub>2</sub> particles have been synthesized using precipitation, sol-gel, emulsion, and bioinspired methods.<sup>50</sup> In this thesis, the monodisperse particles that have been obtained using the Stöber process.

### 2.5.1. Synthesis of Silica Particles Using Stöber Process

TEOS is the origin of silica and hydrolyzed in an alkali medium such as -OC<sub>2</sub>H<sub>5</sub> groups that are easily replaced by -OH, and contributing to silicic acid formation, Si(OH)<sub>4</sub>. Then, silica clouds begin to form by condensation of silicic acid. The silica clouds

reaching the critical mass are about 2-3 nm in size and as a result, nuclei are born. Nuclei are also called insoluble primary particles and larger colloidal particles begin to form with the association of the primary particles due to their aggregation in alkali medium (Figure 2.8) <sup>51</sup>. The resulting SiO<sub>2</sub> colloidal dispersion is white in color.

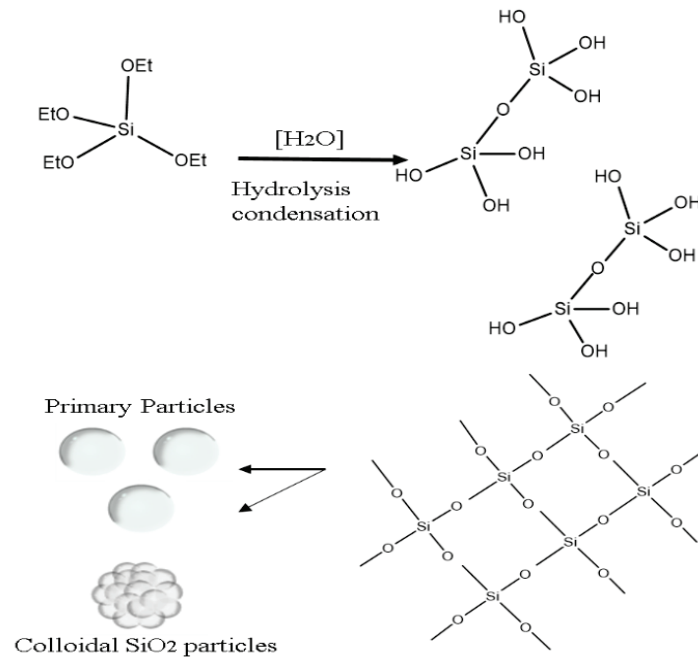


Figure 2.8. Synthesis of silica particles via Stober process.

## CHAPTER 3

### EXPERIMENTAL

#### 3.1. Materials

Tetraethyl orthosilicate (TEOS, 99%), ammonia hydroxide (25% v/v aqueous solution of  $\text{NH}_3 \cdot \text{H}_2\text{O}$ ), hexadecyltrimethylammonium bromide (CTAB), concentrated sulfuric acid ( $\text{H}_2\text{SO}_4$ , 98%), chloroform (99%), methanol ( $\geq 99.9\%$ ), hydrogen peroxide ( $\text{H}_2\text{O}_2$ , 30% v/v aqueous solution), styrene (99%), poly (ethylene glycol) phenyl ether acrylate (PEGPEA), and 2-hydroxy-2-methylpropiophenone (97%) were supplied from Sigma Aldrich. Ethanol ( $> 96\%$ ) and 2- propanol (IPA,  $\geq 99.5\%$ ) were supplied from Tekkim. SYLGARD 184 Silicone Elastomer Kit was purchased from Sigma Aldrich and PDMS used as polymer matrix. The deionized water ( $18.2 \text{ M}\Omega \cdot \text{cm}^{-1}$  at  $25 \text{ }^\circ\text{C}$ ) was supplied by using a Milli-Q Advantage water treatment system.

#### 3.2. Methods

##### 3.2.1. Synthesis of Colloidal Silica Particles

Monodisperse colloidal  $\text{SiO}_2$  particles were synthesized by Stöber method. Initially, the preferred amount of ammonia (from 1 to 2 mL), ethanol (from 20 to 40 mL), and ultra-pure water (from 0.5 to 1 mL) were stirred in glass vessel under sonication. Then, TEOS (1 mL) was added into mixing solution. Afterward, the reaction was permitted until after the opaque white color was converted from a transparent solution. Then the mixture was centrifuged to collect colloidal  $\text{SiO}_2$  particles. During the centrifuge process, colloidal  $\text{SiO}_2$  particles were obtained as a precipitate washed by ethanol with three times to completely remove unreacted TEOS. Eventually, at room temperature, the resulting white powders were dried for 24 h.

### **3.2.2. Surface Modification of SiO<sub>2</sub> Particles**

Colloidal SiO<sub>2</sub> particles surface modification was performed using CTAB as a cationic surfactant for partial hydrophobic properties. Previously, an amount of colloidal SiO<sub>2</sub> particles (0.1 g) was dispersed for 24 h in 5 mL of 2-propanol under sonication, and CTAB (4 mg) was then added to the dispersion. The dispersion was homogenized in 30 minutes under probe sonication (40% amplitude, 1:2 pulse). The dispersion was finally centrifuged three times and washed with IPA to remove unreacted CTAB (6000 rpm, 20 min). CTAB-modified colloidal SiO<sub>2</sub> particles were dried in the vacuum oven at room temperature for about one day. The produced particles were further dispersed in a mixture of chloroform and methanol (4:1, v: v) to spread to the water subphase.

### **3.2.3. Preparation of Glass Substrates**

Microscope glass slide (20 × 20 mm<sup>2</sup>) was used as a substrate for three-layers deposition. First, the slides were carefully cleaned in acetone, ethanol, and deionized water for 10 min. The substrates were then immersed in the mixture of H<sub>2</sub>SO<sub>4</sub> and H<sub>2</sub>O<sub>2</sub> (3:1, v: v) to activate hydroxyl groups. The corresponding substrates were then dried by utilizing nitrogen.

### **3.2.4. Preparation of the Langmuir-Blodgett Films**

Modified colloidal SiO<sub>2</sub> particles were prepared in a mixture of chloroform and methanol (4:1, v: v). The colloidal SiO<sub>2</sub> particles concentration was kept constant (10 mg. mL<sup>-1</sup>) throughout all experiments. The colloidal SiO<sub>2</sub> particles dispersions were homogenized in ultrasonic bath at least half an hour. Then, the produced dispersions were spread on a distilled water surface by using micro syringe. The amount of dispersion was kept constant at 100 μL in all experiments. The solvent was allowed to evaporate for about 45 min before the compression process began. The 2D monolayer compression process was applied at a speed of 1 mm.min<sup>-1</sup>. Depending on the transfer surface pressure, colloidal SiO<sub>2</sub> particles were deposited on the glass substrate at a speed of 1 mm/min in the upstroke direction. Afterward, the deposition process was applied three times to

produce three-layer photonic crystals by LB method. Figure 3.1 shows the SiO<sub>2</sub> synthesis, modification of SiO<sub>2</sub> particles and LB deposition process.

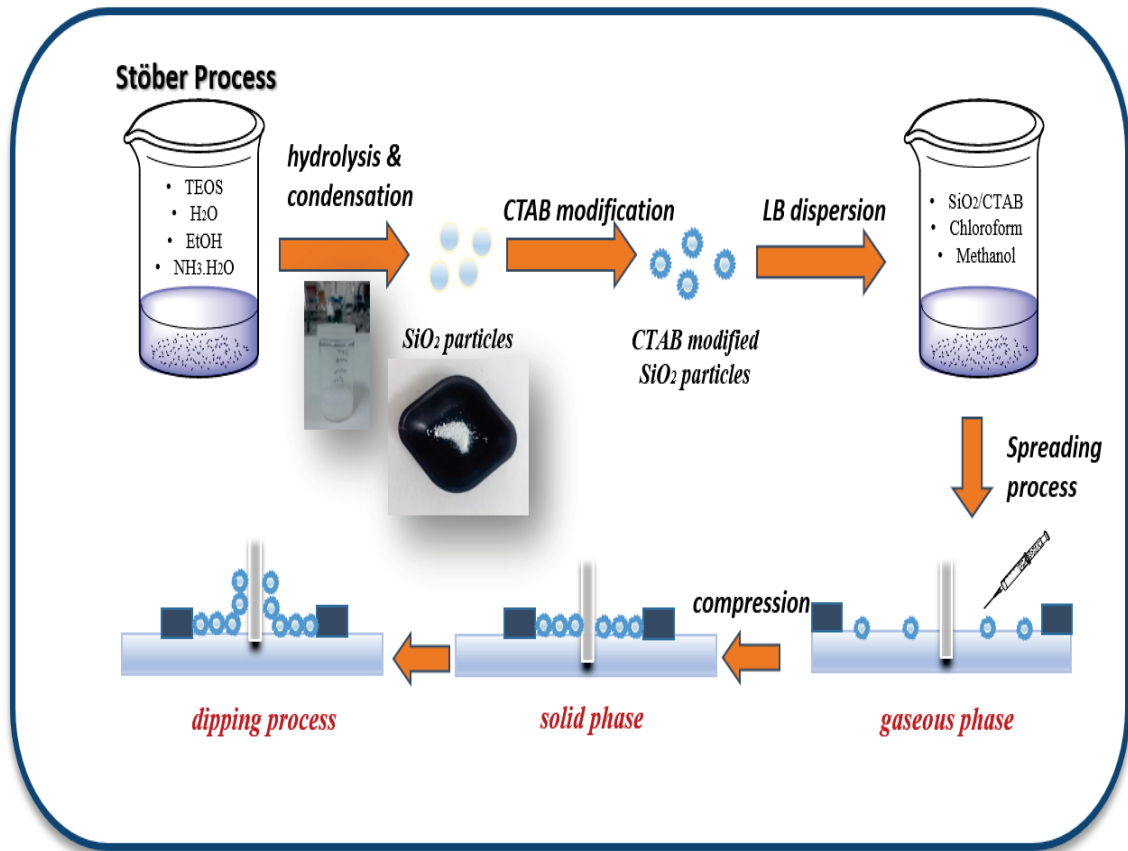


Figure 3.1. Schematic representation of fabrication of the three-layer LB films.

### 3.2.5. Synthesis of Poly (Ethyl Acrylate-Co-Methyl Methacrylate) By Free Radical Polymerization

Poly (ethyl acrylate-co-methyl methacrylate) copolymer was synthesized by free radical polymerization from ethyl acrylate (EA) and methyl methacrylate (MMA) monomers, considering their mechanical stability and hydrophobic property, in addition to their elastomeric properties. The monomers (EA: MMA, 2:1 mole) were dispersed in 15 mL of toluene medium. As the initiator, benzoyl peroxide (BPO) (0.5 mole %) was added to the system. Nitrogen gas was used to remove oxygen in the environment, considering the efficiency of the polymerization. The reaction was stirred for approximately 8 hours at 85° C. The resulting copolymer P (EA-co-MMA) was utilized in the SiO<sub>2</sub>/chloroform dispersion to be used in the Langmuir Blodgett deposition.

### 3.2.6. Fabrication of Elastomer SiO<sub>2</sub>/PDMS Film

The PDMS oligomer and cross-linker (10:1 w %) mixture was poured onto the three-layer photonic crystal film on the glass substrate. The elastomer PDMS film thickness was controlled between 0.5 and 1 mm. Then the setup was cured for 24 h at 60°C. Finally, PDMS/SiO<sub>2</sub> layer was peeled from the glass substrate and elastomer composite film was produced. Figure 3.2 shows the schematic representation of elastomer film production.

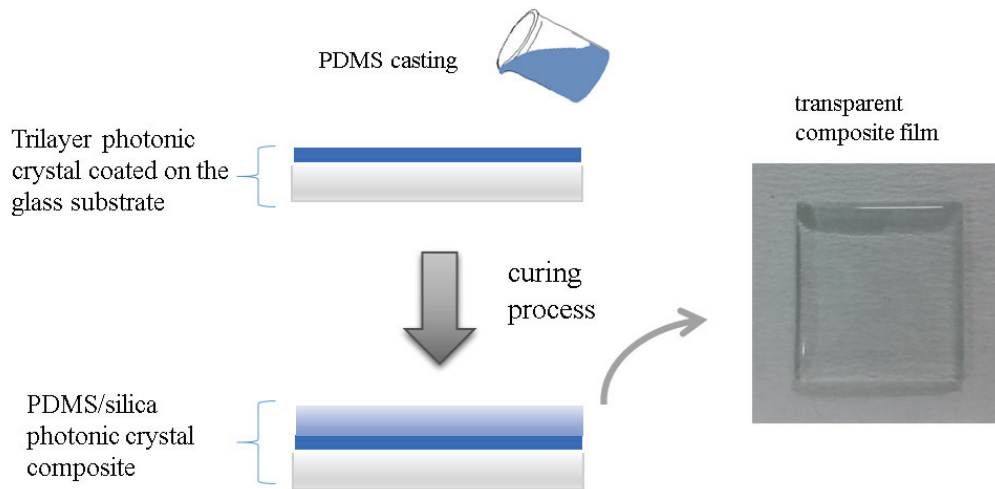


Figure 3.2. Schematic representation of the fabrication of PDMS/ SiO<sub>2</sub> film.

### 3.2.7. Fabrication of Strain Responsive Elastomer SiO<sub>2</sub>/P(PEGPEA) Films

In the presence of photonic crystal films, the strain-responsive elastomers were manufactured by the photopolymerization process. Figure 3.3 shows the schematic illustration of followed method. The produced photonic crystals were placed into space between two glass slides divided by 1 mm thick spacers. The reactive solution was prepared by mixing PEGPEA and photoinitiator (96:4, v: v) and was quickly injected into the gap due to lateral capillary force. It was subsequently allowed to penetrate the solution into voids between colloidal SiO<sub>2</sub> particles for 30 min. UV light irradiated the system for 3 min. The corresponding polymerized composite film was carefully peeled from the glass substrate.



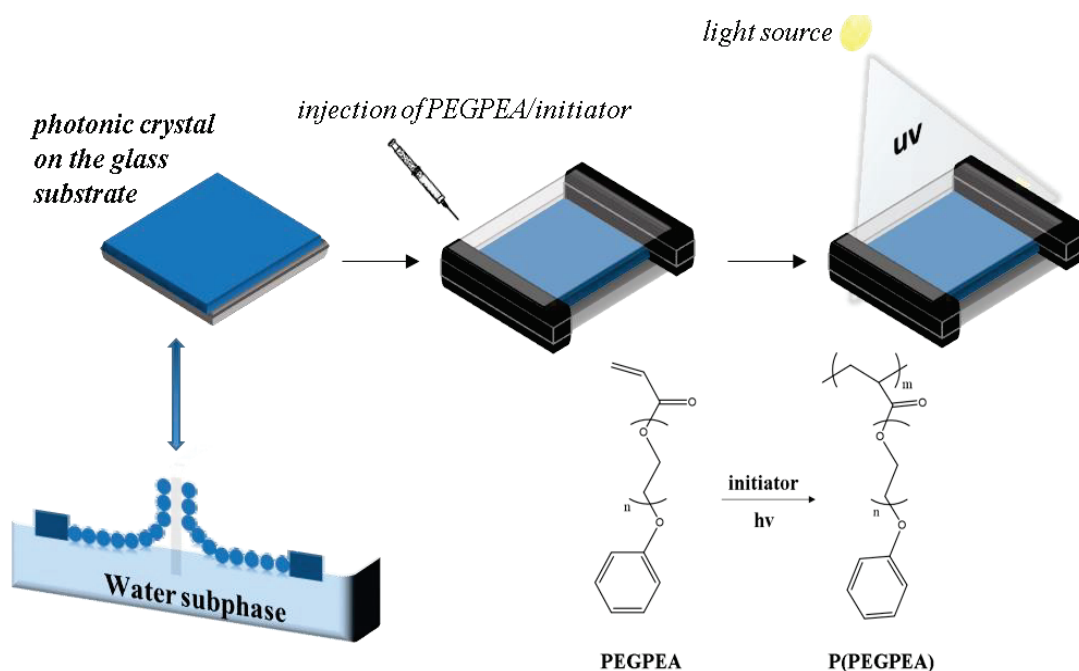


Figure 3.3. Schematic representation of photopolymerization process.

### 3.3. Characterization

The average size and zeta potential of the particles was investigated by using Dynamic Light Scattering (DLS; Zeta sizer Nano ZS, Malvern Instruments, Worcestershire, UK). The morphology of the colloidal particles and composite films was determined by Scanning Electron Microscopy (SEM; Quanta 250, FEI, Hillsboro, OR, USA). The reflection spectra of the photonic films were recorded by spectrometer (USB2000+, Ocean Optics Inc., Dunedin, FL, USA) via premium fiber cable. The photographs of the films were taken with cell phone camera (Apple, iPhone 7, CA, USA).

## CHAPTER 4

### RESULTS AND DISCUSSION

#### 4.1. Synthesis of SiO<sub>2</sub> Colloids

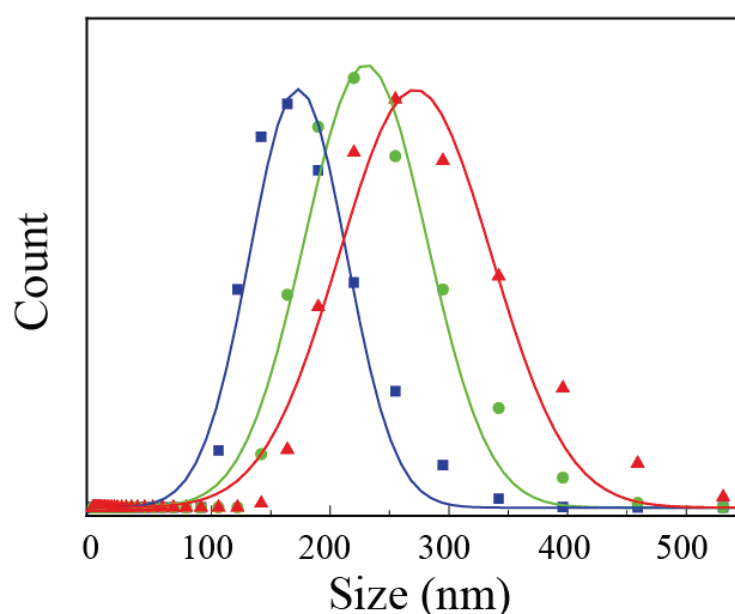


Figure 4.1. DLS size distribution of SiO<sub>2</sub> particles.

Figure 4.1 shows the DLS size distribution of colloidal SiO<sub>2</sub> particles. The size control in the reaction was controlled by TEOS concentration in the system and the amount of water (1 mL) was kept constant. According to DLS results, the size of the particles increases as the concentration of TEOS increases and the resulting sizes are  $175 \pm 10$  nm,  $230 \pm 10$  nm and  $280 \pm 10$  nm, respectively. The polydispersity index (PDI) values of the measured sizes were found to be below 0.05. To summarize these results, (Table 4.1) provides information about synthesized SiO<sub>2</sub> particles and surface modification with the CTAB molecule. This value indicates that the particles synthesized by the Stöber method have uniform size distribution. As a result, it was decided that monodispersed SiO<sub>2</sub> particles were suitable for photonic crystal film applications.

Table 4.1. Detailed information about the resulting colloidal SiO<sub>2</sub> particles; conditions of reaction, size, and zeta potential.

<b>Diameter(nm)</b>	<b>TEOS (mL)</b>	<b>EtOH (mL)</b>	<b>PDI</b>	<b>ζ potential- bare silica (mV)</b>	<b>ζ potential- modified silica (mV)</b>
<i>175± 10 nm</i>	<i>1</i>	<i>30</i>	<i>0.024</i>	<i>-59</i>	<i>-3,56</i>
<i>230±10 nm</i>	<i>1</i>	<i>25</i>	<i>0.048</i>	<i>-35</i>	<i>20,6</i>
<i>280±10 nm</i>	<i>1</i>	<i>20</i>	<i>0.019</i>	<i>-7.9</i>	<i>22,4</i>

## 4.2. Investigation of Various Substrates

The ability of the SiO<sub>2</sub> particles to spread homogeneously on the water subphase is one of the most important conditions required for a successful deposition. In addition, the surface properties of the substrate used during the dipping process are very important for this homogeneous dispersion to be transferred to the film. Therefore, different substrate experiments were made for colloidal SiO<sub>2</sub> particles. In the depositions, glass slide, quartz slide, metal plate (aluminum) and silicone plates were used as a substrate, respectively. In these experiments, firstly, high quality microscope slide, also known as soda-lime glass, was used as the glass substrate. Quartz slides are often used in applications where permeability is important in the ultraviolet region. Glass, quartz and silicon plates were cleaned in the Piranha solution (H<sub>2</sub>SO<sub>4</sub>: H<sub>2</sub>O<sub>2</sub> 3:1) before used. Afterward, all substrates were kept in an ultrasonic bath for 10 minutes with acetone, ethanol and ultrapure water. Figure 4.2 shows the isotherm curves were taken for different substrates. While the isotherm curves are taken, all substrates are immersed in the ultra-pure water (8 mm). The same amount of CTAB/SiO<sub>2</sub> mixture was used in all experiments (100 μL, chloroform/methanol). For each experiment, phase transitions were observed in the isotherm curves, and the transfer pressure to the solid phase was different from each other. The letters are given in each isotherm curve, respectively; "G" gas phase "L" liquid phase "S" represents the solid phase. Initially, it was assumed that spreading particles were in the gaseous phase due to the low attractive forces between each other. Depending on the surface pressure increased with the compression of the barriers, the particles first transferred to the liquid phase and then to the solid phase. Distance between particles decreased during these phase transitions. The transfer pressure to the solid phase is 30,

25, 30, and 22 mN/m for the quartz slide, silicon plate, metal plate and glass slide, respectively.

Figure 4.3 shows the SEM images of the three-layer deposited colloidal SiO<sub>2</sub> particles by using the LB method on the quartz, metal, silicon, and glass substrate surface. Three-layer deposition was applied on each substrate. As a result, the multilayer colloidal SiO<sub>2</sub> particles were transferred successfully onto different substrates. When the SEM image of the metal plate was taken into consideration, it observed that the agglomeration of the colloidal SiO<sub>2</sub> particles was high due to the metal surface roughness. Moreover, it has been observed that the periodic sequence ratio, which forms the regular structure on the silicon plate and quartz surfaces, is higher than that of the metal plate. When the SEM image of the glass substrate surface is examined, it is seen that the colloidal SiO<sub>2</sub> particles have a relatively close packed structure in multiple layers.

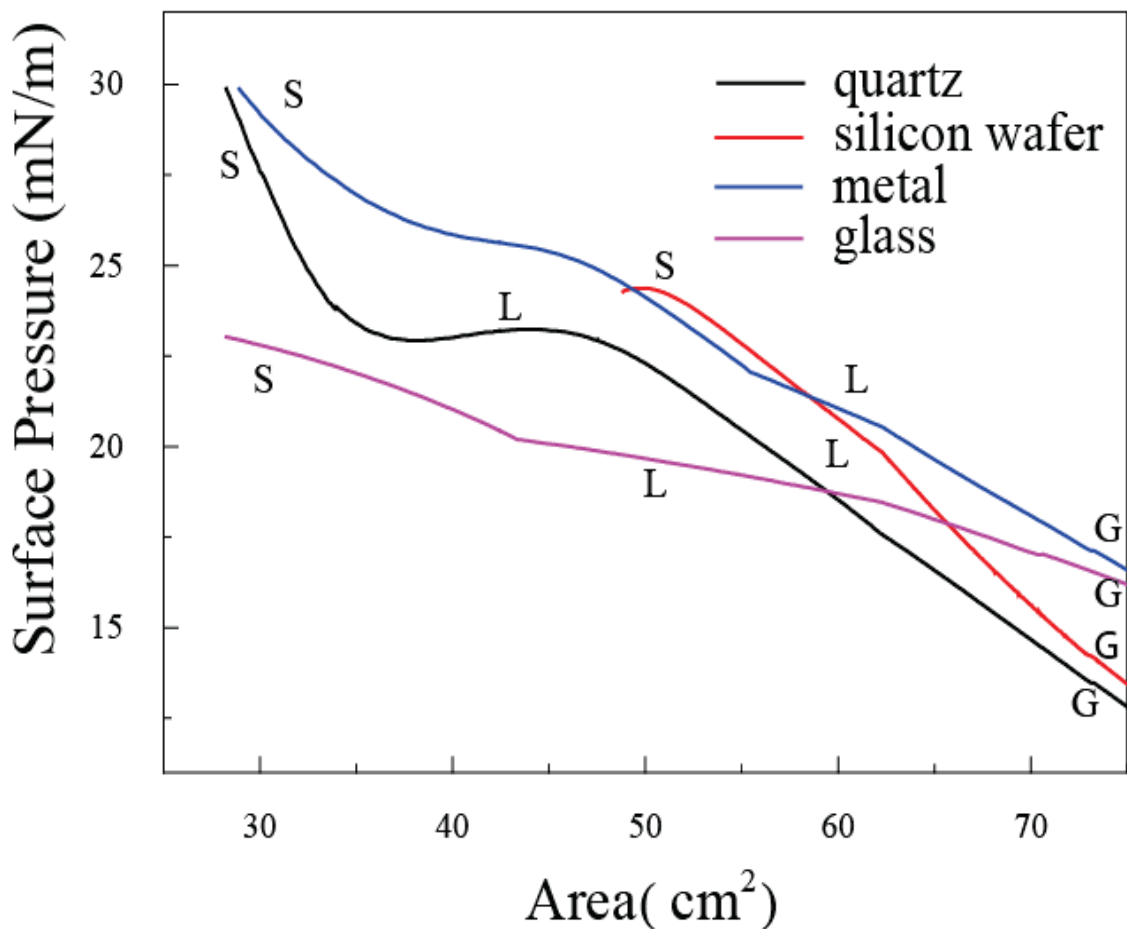


Figure 4.2. Isotherm curves for various substrate.

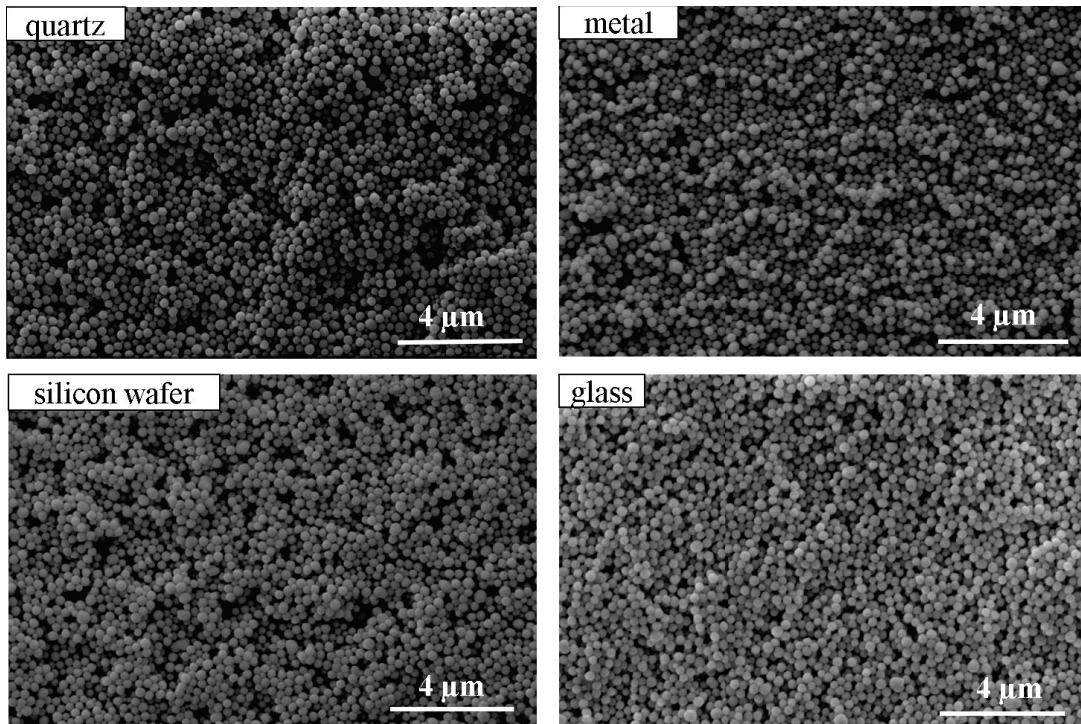


Figure 4.3. SEM images of SiO<sub>2</sub> particles coated with Langmuir Blodgett method on various substrate.

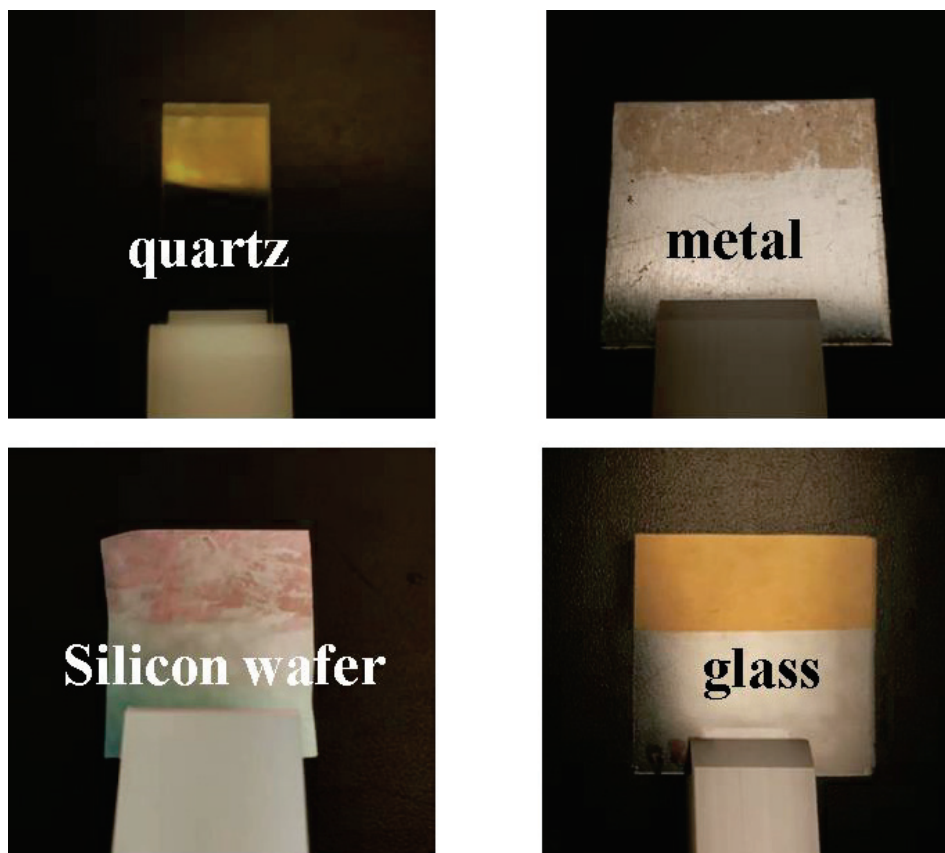


Figure 4.4. Photographs of various substrates coated with three-layers of SiO<sub>2</sub> colloids.

Figure 4.4 shows photographs of three-layer colloidal SiO<sub>2</sub> particles on different substrates. According to the photographs of the films, it was observed that the quartz and the glass surface had a more homogenous coating and higher color saturation compared to the metal and silicon substrates. Due to the transparent nature of the quartz and glass surfaces, the resulting yellow color can be easily distinguished.

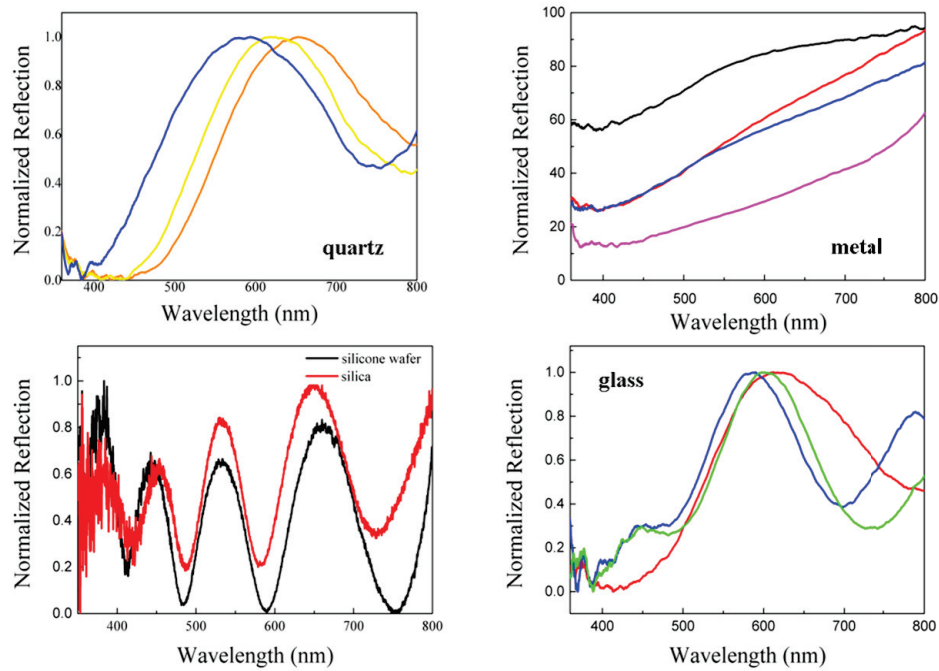


Figure 4.5. Reflection spectra of three-layer SiO<sub>2</sub> particles with various substrates.

Figure 4.5 shows the normalized reflection spectra of colloidal SiO<sub>2</sub> particles deposited on four different substrates. According to the obtained spectra, it was decided the type of substrate surfaces that would be more suitable for the production of photonic crystal films. When the normalized reflection spectrum of the three-layer colloidal SiO<sub>2</sub> particles on quartz substrate is observed, it is found that the maximum reflection wavelengths range from 655 to 584 nm depending on the increasing angle. Spectra also showed that the color was shifting to blue in the visible region. This shift in the spectrum also confirms the Bragg-Snell law. Therefore, the three-layer colloidal SiO<sub>2</sub> particles deposited on the quartz substrate are suitable for use in photonic crystal applications due to their ability to change color depending on the angle. When the spectrum of aluminum metal surface was examined, no information could be obtained from the spectrum due to the high reflectivity of metal although the colloidal SiO<sub>2</sub> particles were transferred to the metal surface. Therefore, the metal substrate is not suitable for production of photonic

crystal film. In view of the normalized reflection spectrum of the silicone substrate, reflection signals are recorded from both silicones surface itself and the colloidal SiO<sub>2</sub> particles deposited on the surface. Since the reflection signal from the silicon substrate is very severe, a distinct color spectrum could not be obtained from the film surface. Lastly, observed in the quartz substrate, the reflection spectrum of the colloidal SiO<sub>2</sub> particles deposited on the glass substrate showed that the normalized reflection wavelength shifted towards the blue region due to the increased angle. As a result, the experiments achieved from different surface of the substrates. It has been decided that quartz and glass substrate surfaces were suitable for the production of photonic crystal films for using in the Langmuir Blodgett method. The integration of photonic crystal films into polymer matrices will be investigated in future studies; hence, the substrate used must be highly resistive to breakage, deformation and cost-effective. As a result, the studies were continued with the glass substrate.

### **4.3. Langmuir Blodgett Films and Their Elastomeric Matrix Composite**

The integration of the photonic crystals obtained by the LB method to the polymer matrix was performed. In this context, various integration methods were carried out such as drop casting process, photopolymerization process, monomer/SiO<sub>2</sub>, and polymer/ SiO<sub>2</sub> LB deposition. The first one of these methods is monomer/SiO<sub>2</sub> deposition by the LB method. Photonic crystal film was prepared by using vinyl monomers in the silica dispersion and the optical properties of the films were investigated. In the second method, an elastomeric poly (ethyl acrylate-co-methyl methacrylate) was synthesized by solution polymerization. The synthesized polymer was dispersed in SiO<sub>2</sub>/chloroform dispersion and coated with Langmuir Blodgett method onto the glass substrate. Unfortunately, polymer/SiO<sub>2</sub> and monomer/SiO<sub>2</sub> depositions are unsuccessful due to high aggregation of the colloidal SiO<sub>2</sub> particles. In the third method, poly(dimethylsiloxane) (PDMS), which is a flexible polymer as a matrix material, was chosen. Later on, elastomer composite films were produced by drop casting method. PDMS were used an elastomer matrix for composite films. In the fourth method, the SiO<sub>2</sub> photonic crystal films obtained by LB method were combined with the monomer with capillary force and the elastomer composite films were generated by the photopolymerization.

#### 4.4. Monomer/Silica Monolayers Produced from Different Vinyl Monomers

To produce photonic crystalline films having elastomeric properties, various monomers with colloidal SiO<sub>2</sub> particles were used as a reactive dispersant. Firstly, the excess number of monomers was used to dissolve in the SiO<sub>2</sub>/chloroform dispersion by using an ultrasonic bath. Then, the resulting films were exposed to UV light to produce polymer composite films. Styrene and poly (ethylene glycol) phenyl ether acrylate (PEGPEA) were used as a monomer. Monomer/SiO<sub>2</sub> dispersions were kept in the ultrasonic bath at least 30 min to minimize aggregation. The colloidal particles dispersions were spread on ultrapure water subphase by using a micro syringe followed by a 10 min waiting period for solvent evaporation. Then, the monomer/ SiO<sub>2</sub> dispersion monolayer was compressed at a speed of 3 mm.min<sup>-1</sup> and the particles were deposited at the chosen surface pressure at the same speed of 1 mm.min<sup>-1</sup> in the upstroke direction.

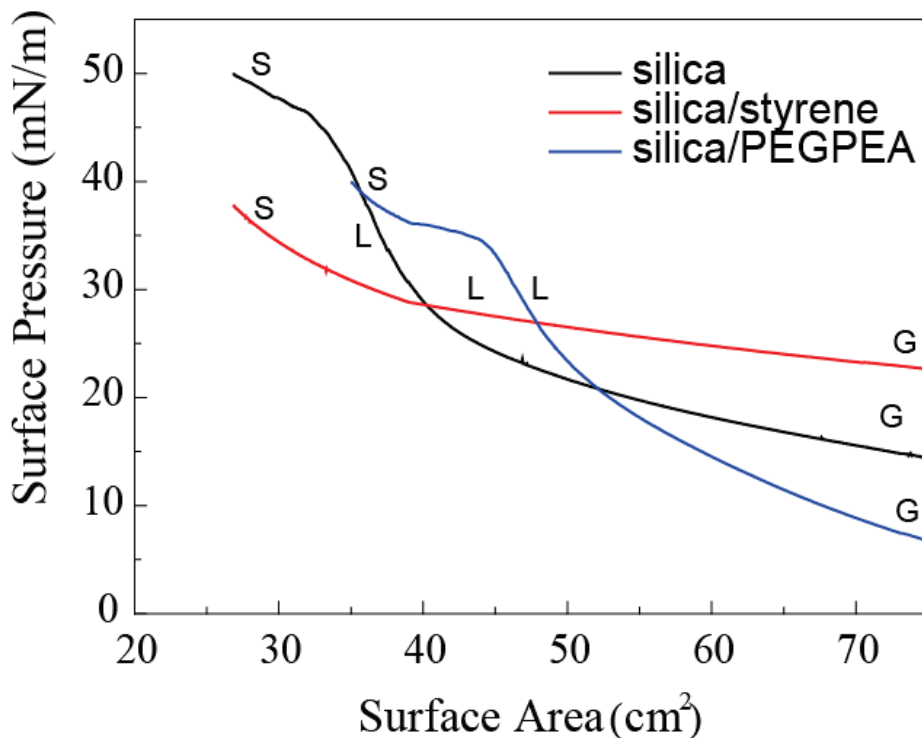


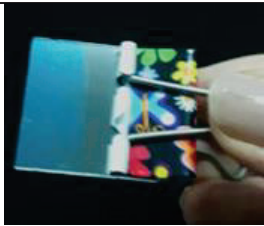


Figure 4.6. Isotherm curves of different monomer/ SiO<sub>2</sub> dispersions.

The isotherm curves of different monomer/SiO<sub>2</sub> composites were obtained by compression of the barriers are given in Figure 4.6, respectively. When the isotherm of



the bare SiO<sub>2</sub> was examined, the two-dimensional film initially assumed to be in the gaseous phase and it was transferred to the solid phase about 50 mN/m. When the isotherm curves of SiO<sub>2</sub>/styrene and SiO<sub>2</sub>/PEGPEA dispersions are examined, the pressures to be transferred to the solid phase were 38 mN/m and 40 mN/m, respectively. Then, the monolayers of dispersions were transferred to the glass substrates. The resulting films were cured under UV light source for 3 min. The film contains bare SiO<sub>2</sub> was more homogeneously coated on the glass substrate than the monomer containing films. The films of monomer/ SiO<sub>2</sub> were not homogeneously spread into the water surface due to their aggregation and spreading of droplet-like shape. On the other hand, monolayer films exhibited angle-independent structural color due to non-close packed array. Because of the high aggregation of monomer-containing films, it was understood that they were not suitable for photonic crystal elastomer composite applications. Table 4.2 shows the parameters used in SiO<sub>2</sub>/ monomer depositions and results.

Table 4.2. Parameters of monomer/SiO<sub>2</sub>coating and results.

<b>Materials</b>	<b>Spreading amount ( μl)</b>	<b>Transfer Pressure (mN/m)</b>	<b>Properties of the produced films</b>	<b>Photographs</b>
SiO <sub>2</sub>	100	50	Blue color Homogeneous distribution	
SiO <sub>2</sub> -styrene	100	40	Blue color Agglomeration	
SiO <sub>2</sub> -PEGPEA	100	40	Blue color Agglomeration	

#### 4.5. Polymer/Silica Monolayers

In the second method, the polymer was directly dissolved into the SiO<sub>2</sub>/chloroform dispersion. For this purpose, poly (ethyl acrylate-co-methyl methacrylate) copolymer was synthesized by free radical polymerization. Firstly, the polymer/SiO<sub>2</sub> dispersion was coated on the glass substrate by LB method. Then, synthesized polymer was used for second time and cast onto the polymer/SiO<sub>2</sub> LB film to increase thickness of the film.

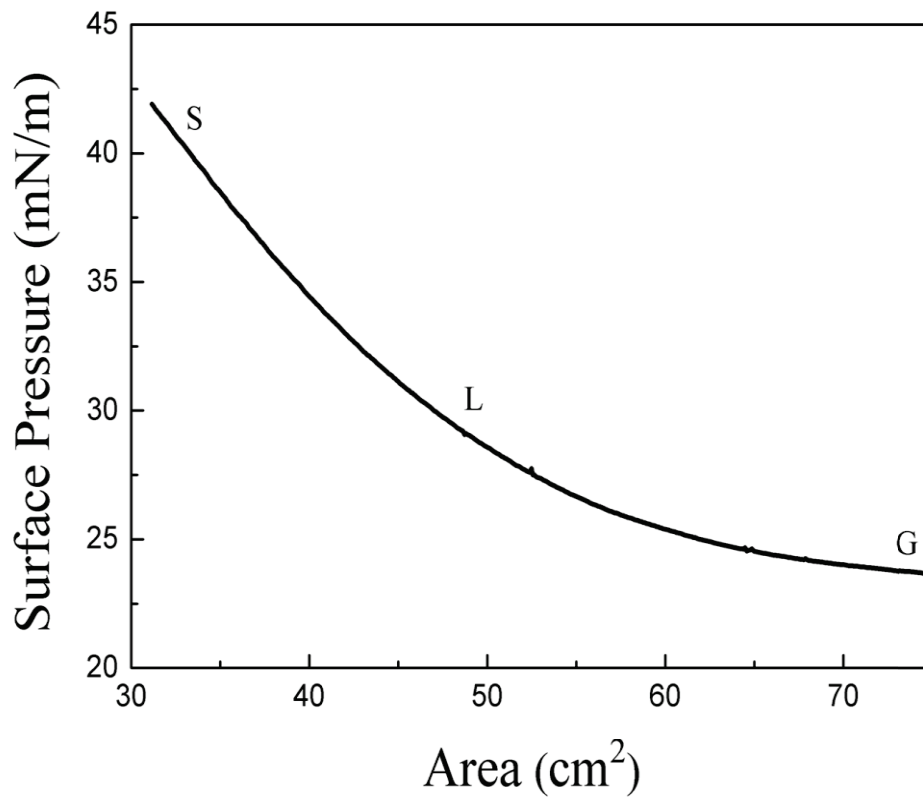


Figure 4.7. Isotherm curve of polymer/ SiO<sub>2</sub> dispersion.

The 30 mg of P (EA-co-MMA) polymer was dispersed in a mixture of SiO<sub>2</sub> / chloroform (10 mg / mL). Ultrasonic stirrer was used to dissipate of particles (30 min). The resulting mixture was dispersed on the water phase in a volume of 200  $\mu$ L. The waiting time was kept short (15 min) to minimize agglomeration. According to the obtained isotherm curve, it was assumed that the mixture, which was initially accepted in the gas phase, passed the solid phase at about 44 mN/m with the compression of the barriers (Figure 4.7.). After this step, the mixture of P (EA-co-MMA)/SiO<sub>2</sub> was

transferred to the glass substrate. The waiting time was kept about 15 min to minimize aggregations. The waiting time was kept about 15 min to minimize aggregations. According to the obtained isotherm curve, the mixture is assumed to pass the solid phase at about 44 mN /m with the compression of the barriers, which is initially accepted in the gas phase.

P(EA-co-MMA)/toluene solution was poured on the coated film to thicken the film and improve its mechanical properties. The material was fluidized in an oven maintained at 105 °C. At this stage, the polymer was intended to penetrate the P(EA-co-MMA)/SiO<sub>2</sub> film spacers. After waiting for about 30 min, the polymer film was produced by cooling to room temperature at a thickness of about 1 mm.

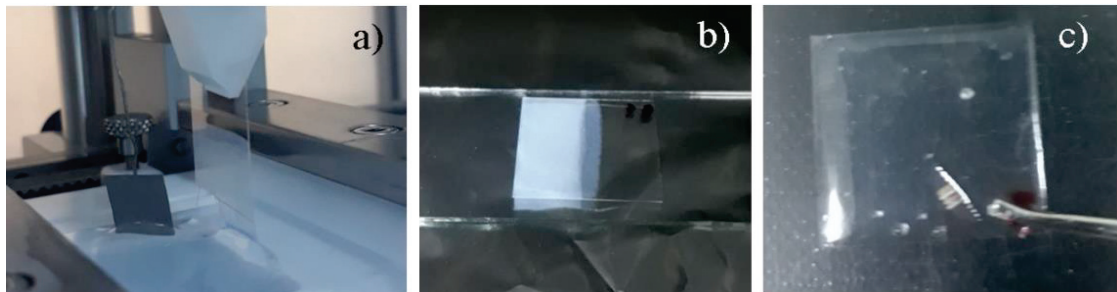


Figure 4.8. Photograph of P (EA-co-MMA)/ SiO<sub>2</sub> dispersion (a) during LB coating, (b) LB coated image, (c) P (EA-co MMA) film casting on film.

Figure 4.8 shows the photograph of the transferring process which is achieved by LB process of the P(EA-co-MMA). The color saturation is low compared to the monomer/SiO<sub>2</sub> films and the composite film of polymer/SiO<sub>2</sub> was transparent (Figure 4.8. (a-b)).

Figure 4.9 shows the SEM and AFM images of P (EA-co-MMA)/SiO<sub>2</sub> film. The resulting Colloidal SiO<sub>2</sub> particles were embedded in the polymer matrix. According to SEM images, the P (EA-co-MMA)/SiO<sub>2</sub> films do not have a homogeneous distribution and colloidal particles are formed as an agglomerate within the polymer matrix. However, due to the high aggregation and the complete deterioration of the photonic crystal structure, the film has an elastomeric structure, but structural coloration was not observed. In a comparable manner, AFM images show that the periodic structure is destroyed due to the agglomeration of colloidal SiO<sub>2</sub> particles in the polymer matrix. Moreover, there are void formations on the surface of the glass substrate. Therefore, it may be said that agglomerations prevent to the complete transferring process.

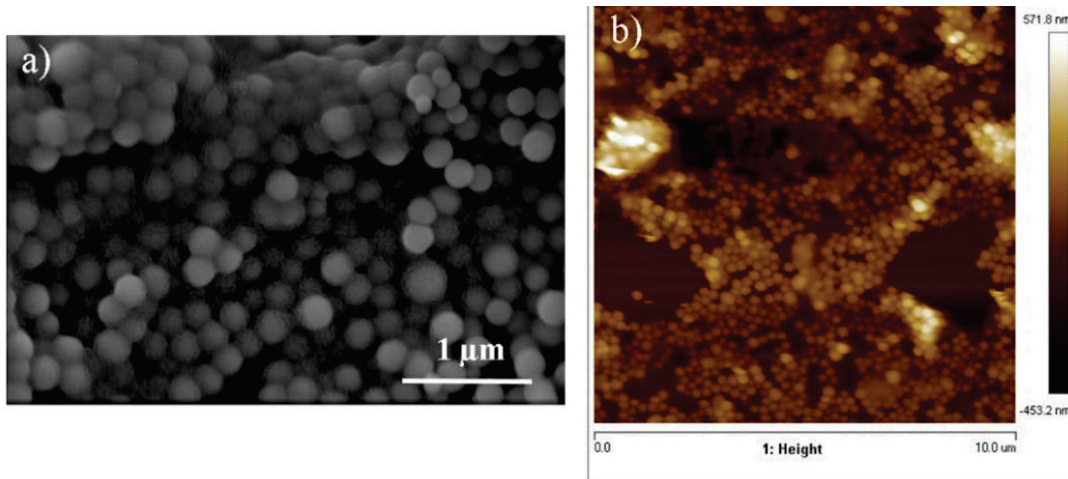


Figure 4.9. (a) SEM image of the thick layer polymer /SiO<sub>2</sub> coating, (b) AFM image of the polymer/silica coating deposited with LB method.

#### 4.6. PDMS/SiO<sub>2</sub> Elastomer Composite

In this period, colloidal SiO<sub>2</sub> particles synthesized by Stöber method. Then three-layer colloidal SiO<sub>2</sub> particles deposited on the glass substrate by LB method. The resulting photonic films exhibit structural coloration. Then particles were embedded to PDMS matrix to procure polymer photonic composites. The refractive index of PDMS (1.425) is very proximate to that of SiO<sub>2</sub> (1.457 @ 632 nm). Therefore, the composite films were highly transparent in the visible region shown in Figure 3.2.

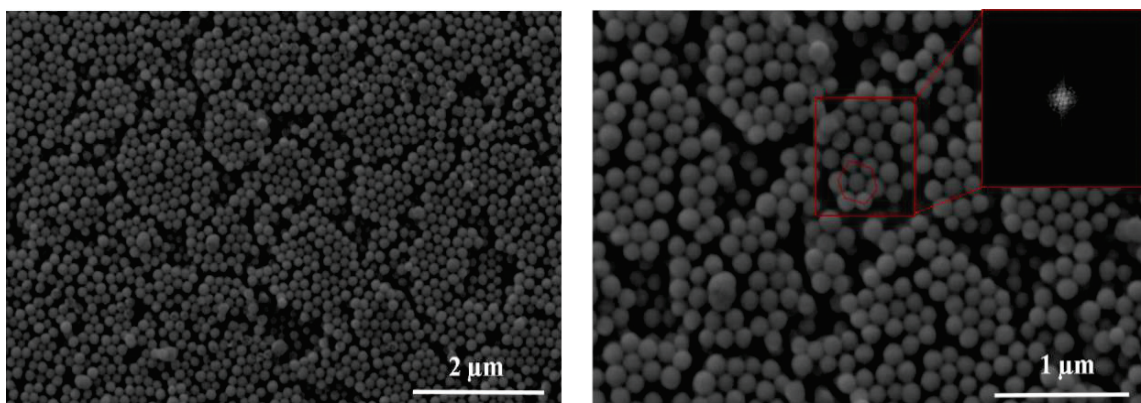


Figure 4.10. SEM images of three-layers SiO<sub>2</sub> particles produced by the Langmuir Blodgett method.

SEM images of three-layer coated colloidal SiO<sub>2</sub> particles on glass substrate by LB method are shown in Figure 4.10. In the SEM images, it could be said that the

colloidal SiO<sub>2</sub> particles are in a periodic order and their structure is similar to the hexagonal close package structure (hcp). Using ImageJ software, Fast Fourier Transform (FFT) is running through this SEM image to unambiguously evaluate structural order. This process converts a given image's geometric structure from a spatial to a frequency domain. Thus, obtaining sharp spots specifying the presence of structural periodicity in certain frequencies. In the resulting frequency distribution, sharp spots were observed. This result indicates that close packed ordered formation of the colloidal SiO<sub>2</sub> particles achieved by using LB deposition method. In addition, the regions marked with red lines indicate the domains of HCP structure. In the resulting frequency distribution, sharp spots were observed. This result indicates that close packed ordered formation of the colloidal SiO<sub>2</sub> particles achieved by using LB deposition method.

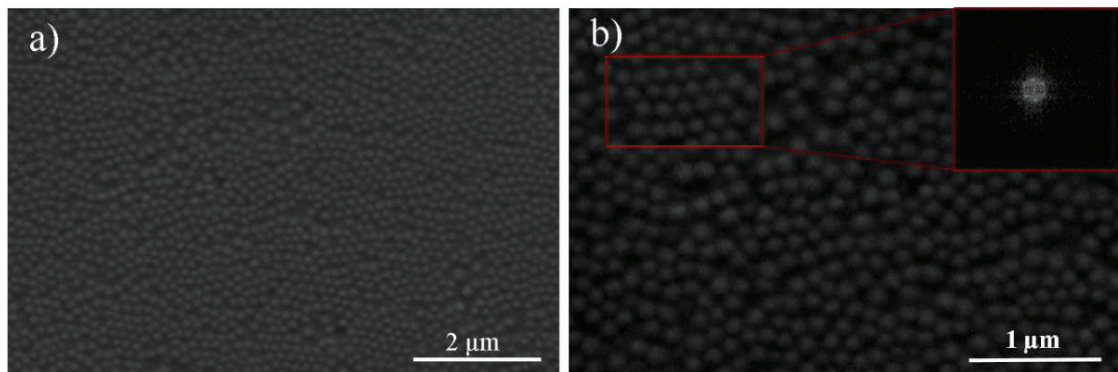


Figure 4.11. SEM images of SiO<sub>2</sub>/ PDMS elastomer (Inset: FFT image of polymer film).

Figure 4.11 (a-b) show the SEM image of the PDMS/SiO<sub>2</sub> elastomer. Without disturbing the SiO<sub>2</sub> structure, the colloidal SiO<sub>2</sub> particles were transferred to the polymer matrix. FFT images show that there is no deterioration of regular structure in the polymer matrix.

Figure 4.12 shows the transmittance spectrum of SiO<sub>2</sub>/PDMS film when strain process is applied. In the initial state, the transmittance of the elastomer film appears to be very high, depending on the spectrum received. As could be recognized from the spectrum, the acquired elastomer film appears transparent. Because the PDMS refractive index ( $n$ : 1.425 at 632 nm) is very close to the refractive index of SiO<sub>2</sub> ( $n$ : 1.457 at 632 nm). When stretching is applied, transmittance is also high (approximately 100%). These results indicate that PDMS elastomer matrix is not suitable for structural colored three-layer photonic crystal produced by LB technique.

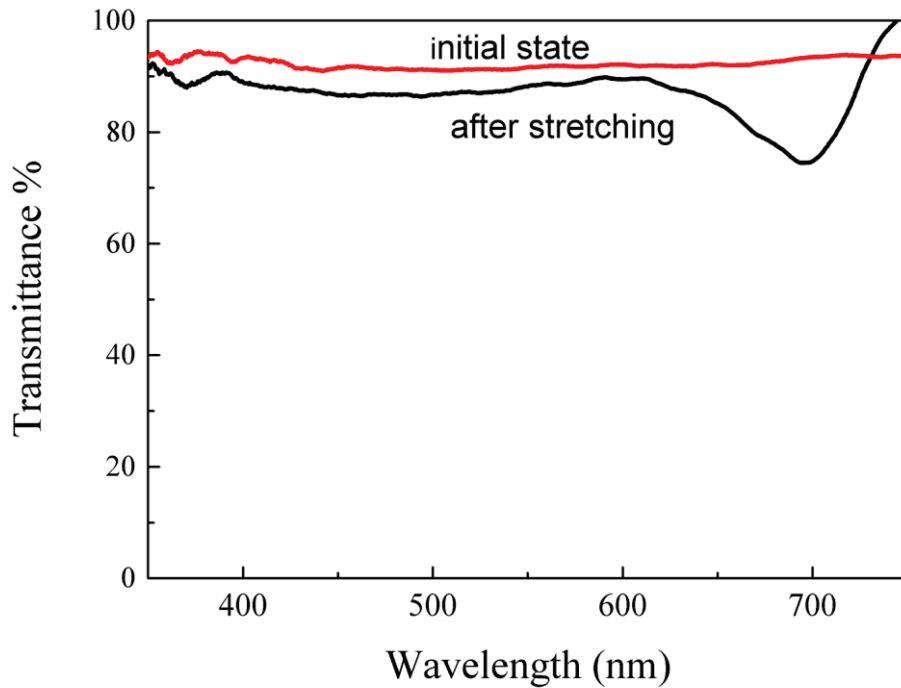


Figure 4.12. Transmittance spectrum of SiO<sub>2</sub>/PDMS composite before and after strain.

## 4.7. Elastomer P(PEGPEA)/Silica Photonic Crystal

### 4.7.1. Three-Layers Photonic Crystals

In order to obtain an elastomer P(PEGPEA)/SiO<sub>2</sub> structure, the photopolymerization method has been performed. The production diagram of structural colored elastomers was shown in Figure 3.3 Three-layer Colloidal SiO<sub>2</sub> particles were coated with the LB deposition method to procure photonic crystal. Surface modification with CTAB provides partially hydrophobic Colloidal SiO<sub>2</sub> particles as well as enhancing particle interactions to achieve 2D monolayer on the water surface.

Figure 4.13 demonstrates that the isotherm curves of colloidal SiO<sub>2</sub> particles are 175, 230, and 280 nm, respectively. The compression ability of monolayer is very important for SiO<sub>2</sub> films to be arranged in the close-packed hexagonal structure. It assumed that the colloidal SiO<sub>2</sub> particles initially spreading on the air-water interface are gaseous phase according to the three different isotherm curves. This assumption indicates that the interactions between the spreading colloidal SiO<sub>2</sub> particles are quite low and that the particles are distant from each other. The particles of different sizes compressed in the same parameters were subsequently transferred to the monolayer at different surface pressures. The transfer pressures of 175 nm, 230 nm and 280 nm diameter monolayer

colloidal SiO<sub>2</sub> particles are 35 mN / m, 24 mN / m, 30 mN / m, respectively. Multilayer SiO<sub>2</sub> photonic crystals have been produced that use the same transfer pressure values. As a result, three-layer colloidal SiO<sub>2</sub> particles were deposited on the glass substrate using the LB method.

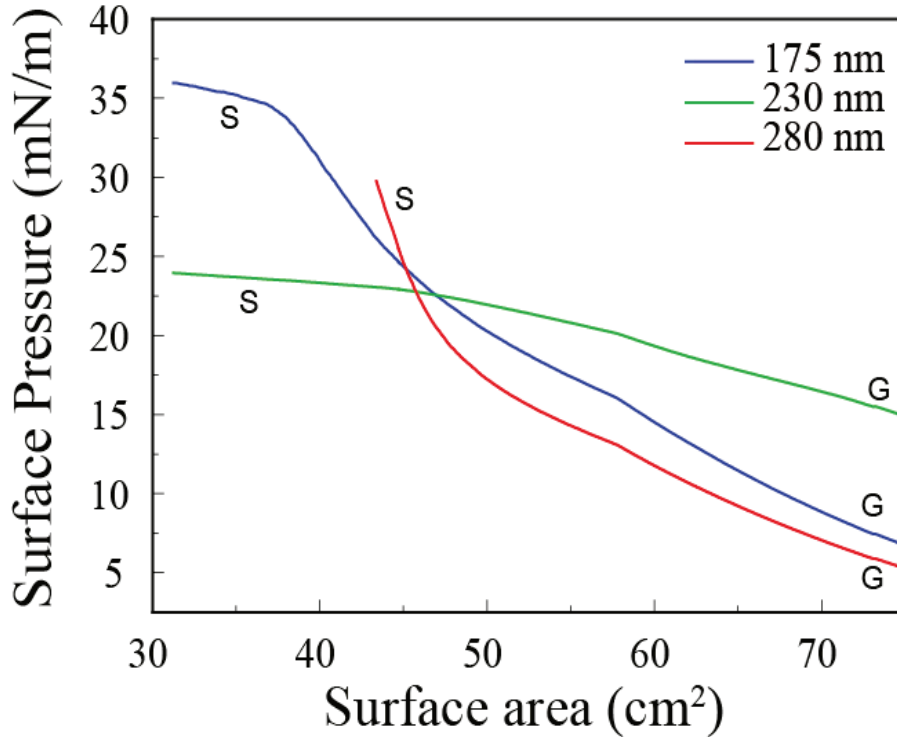


Figure 4.13. Isotherm curves of three-layers SiO<sub>2</sub> particles.

Figure 4.13 demonstrates that the isotherm curves of colloidal SiO<sub>2</sub> particles are 175, 230, and 280 nm, respectively. The compression ability of monolayer is very important for SiO<sub>2</sub> films to be arranged in the close-packed hexagonal structure. It is assumed that the colloidal SiO<sub>2</sub> particles initially spreading on the air-water interface are in the gaseous phase according to the three different isotherm curves. This assumption indicates that the interactions between the spreading colloidal SiO<sub>2</sub> particles are quite low and that the particles are distant from each other. The particles of different sizes compressed in the same parameters were subsequently transferred to the monolayer at different surface pressures. The transfer pressures of 175 nm, 230 nm and 280 nm diameter monolayer colloidal SiO<sub>2</sub> particles are 35 mN / m, 24 mN / m, 30 mN / m, respectively. Multilayer SiO<sub>2</sub> photonic crystals have been produced that use the same transfer pressure values. As a result, three-layer colloidal SiO<sub>2</sub> particles were deposited on the glass substrate using the LB method.

#### 4.7.2. Morphological Properties of Three-Layers LB Films

In this study, chloroform and methanol were used as solvents for the solution spreading to the surface of the LB water subphase. The solvent affects particle wetting behavior in the air / water interface, thus influencing counter ion cloud creation throughout the particles. The hcp arrays of the colloidal particles are clarified by the long-range attraction in constrained geometries and concentrated suspensions between identically charged particles under special conditions.<sup>52</sup>

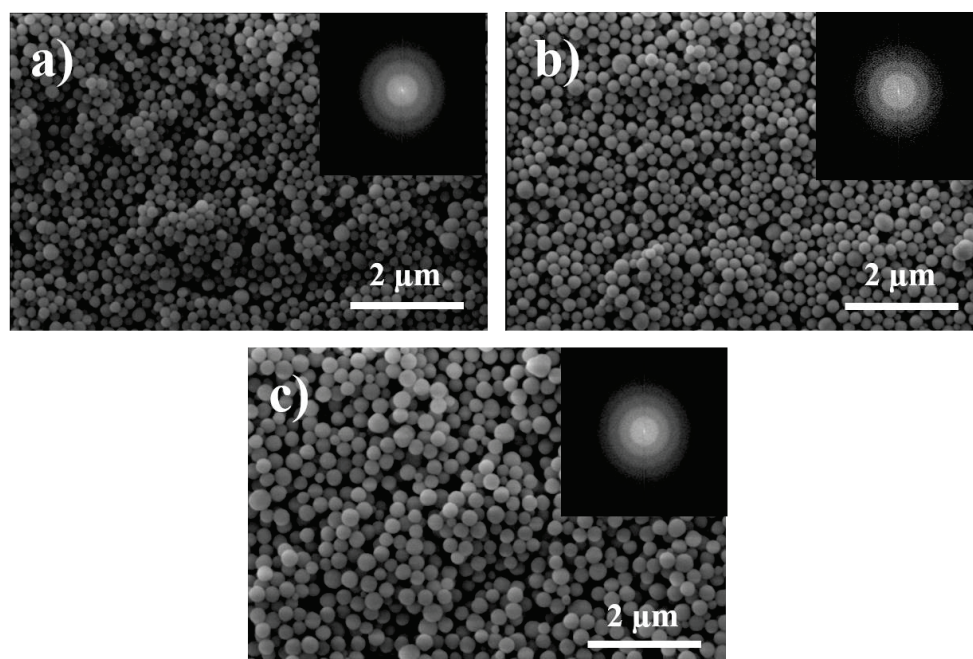


Figure 4.14. SEM images of three-layers SiO<sub>2</sub> particles produced by LB method (Inset: corresponding FFT images).

Figure 4.14 shows the SEM images of three-layer colloidal SiO<sub>2</sub> particles coated at different surface pressures depending on the particle diameter from chloroform-methanol dispersions. The SEM images show that the colloidal SiO<sub>2</sub> particles were successfully transferred to the glass substrate using the Langmuir Blodgett deposition process. The choice of methanol as the co-solvent results in a denser and close-packed monolayer relative to the single solvent system. Likewise, this close-packed structure can be seen from the SEM images of multilayer colloidal SiO<sub>2</sub> particles. In the isotherm curves, the appropriate pressure values were selected and multilayer systems provided the formation of the largest hexagonal closed-packed structure. 2D Fast Fourier Transform



(FT) patterns of SEM pictures are processed and provided as insets to quantify the ordering and the average distance between the particles. The concentric circles of patterns indicate that the films have short range periodic order rather than complete crystal structure. The number of circles hints about the magnitude particle correlation in space.<sup>53</sup> As a result, this periodicity correlation extends over approximately 3 particles for smaller sized spheres (175 and 230 nm), whereas it is 4 particles for the largest one (280 nm).

The particle radial distribution functions were calculated utilizing 16 distinct circles ( $r$ : 3.5  $\mu\text{m}$ ) from the associated with the SEM images. Figure 4.15 (a-b) show that the representative circle and corresponding plots of resulting functions. The intensity of the signals decreases as the radius increases, which also suggests the short-range order of colloidal array. Therefore, it can be concluded that the resulting three- layer films have short-range ordered and non-close packed structures. It may be remarked that the ordering degree is equal or larger than three particles, thus, the three- layer of colloidal arrays may vertically persist their periodicity.

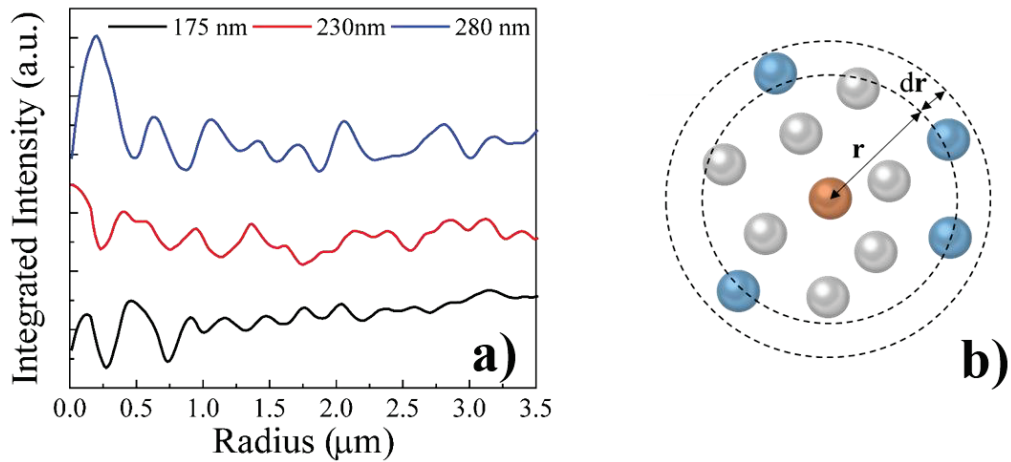


Figure 4.15. (a) Calculated radial distribution functions of colloidal arrays and (b) its schematic representation

Figure 4.16 shows that AFM image of 2D and 3D images of the three-layer colloidal SiO<sub>2</sub> particles, which illustrates hexagonal close packed arrays and periodic arrangement. Additionally, the 3D image provides information on the surface roughness of the structure. The difference in height between the colloidal SiO<sub>2</sub> particles in the surface layer falls to about 100 nm. As a consequence, this height difference is less than the particle size of the colloidal SiO<sub>2</sub> particles (230 nm) and the roughness of the surface may give an idea of the structure forming non-close-packed.

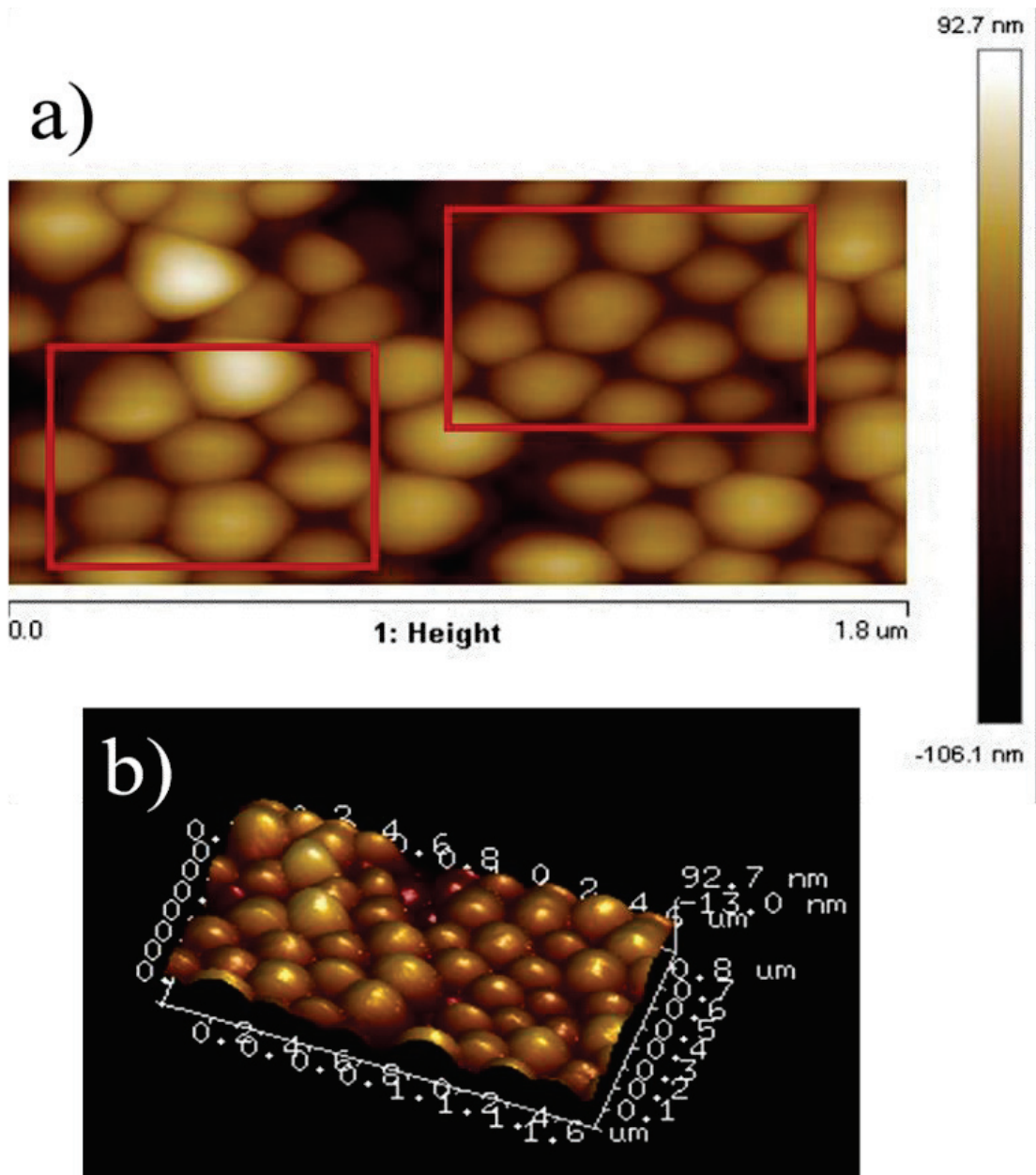


Figure 4.16. AFM image of three-layers photonic crystal, (a) 2D and (b) 3D image.

### 4.7.3. Optical Properties of Three-Layers LB Films

The maximum wavelength peaks vary depending on the incident angle and film diameter. These optical properties are called iridescent. This optical change is expressed by the Bragg-Snell law;

$$\lambda_{max} = 2d_{(111)}\sqrt{(n_{eff}^2 - \sin^2\theta)} \quad (11)$$

The reflected light's wavelength depends on the angle of incident, the lattice spacing of the close-packed structure and the effective refractive index. The lattice spacing of the periodic structure is equal to

$$d_{111} = \left(\frac{\sqrt{3}}{2}\right) D \quad (12)$$

The effective refractive index is termed an additive depending on the volume fraction of SiO<sub>2</sub> particles and air. In the present study, refractive index of the SiO<sub>2</sub> particles ( $n_{silica}$ ) is 1.46 and refractive index of air ( $n_{air}$ ) is 1.0 at 632 nm. Also, the volume fraction of the fcc or hcp structure is 0.74 for photonic crystals.<sup>54</sup> Considering this information, an effective refractive index of spherical colloidal SiO<sub>2</sub> particles has been calculated.

$$n_{eff} = \left(n_s^2 f_s + n_{air}^2 (1 - f_s)\right)^{1/2} \quad (13)$$

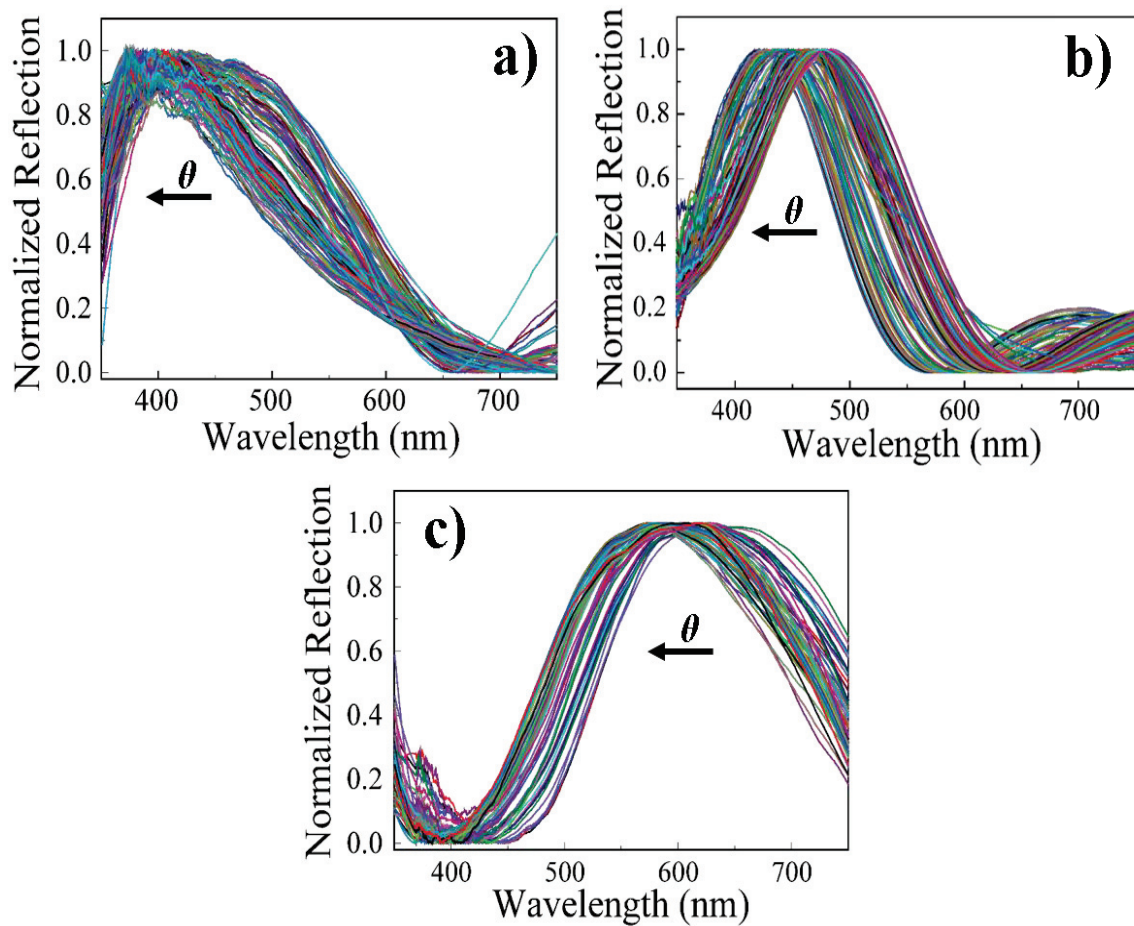


Figure 4.17. Reflection spectra of photonic crystal films with various diameter, (a) 175 nm, (b) 230 nm, (c) 280 nm respectively.

Figure 4.17 shows the reflection spectra of the photonic crystal films produced. Because of the increase in the incident angle, blue shifting was observed in the maximum reflection wavelength ( $\lambda_{max}$ ). This shift was demonstrated in photonic films with three different sizes of colloidal SiO<sub>2</sub> particles. Bragg-Snell law was used to determine the theoretical values of reflection wavelengths. Theoretically,  $\lambda_{max}$  is changing incident angle that shifts from 400 to 265 nm when the diameter is 175 nm. Likewise, the wavelength changes from 530 to 350 nm and from 625 to 415 nm for the particle diameters of 230 and 280 nm, respectively. The maximum value shifts from 430 nm to 370 nm in the reflection spectrum of colloidal SiO<sub>2</sub> particles with a size of 175 nm depending on the various angle. In the photonic film with a diameter of 230 nm colloidal SiO<sub>2</sub> particles, wavelengths shift from 490 nm to 420 nm. In the last calculation, the reflection wavelength shifts from 645 to 575 nm depending on increasing angle when the diameter of colloidal SiO<sub>2</sub> is 280 nm.

Taking into account the corresponding reflection spectra, blue shift is examined based on the increasing angle. However, this shift corresponds to a higher wavelength in experimental results compared to the theoretical calculations (shifting difference of approx. 40 nm). The  $fs$  value for hcp structures is 0.74.<sup>54</sup> The theoretical calculations were made on the basis of this value. On the other hand, the  $fs$  values of the photonic films produced using the LB method are expected to be lower than 0.74 as they do not have a completely close-packed structure. In terms of photonic films with a non-close packed structure, the interplanar distance value is higher than films with close-packed structures. Ultimately, the ( $\lambda_{max}$ ) from the experimental values is higher than the theoretical values.

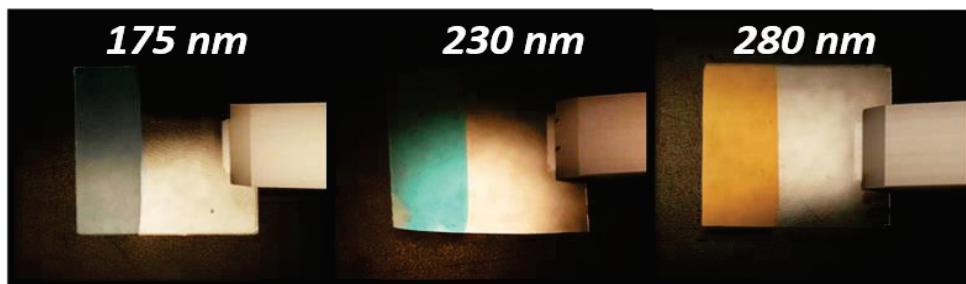


Figure 4.18. Photographs of three-layers SiO<sub>2</sub> films with various diameter.

Figure 4.18 shows that photographs of three-layer SiO<sub>2</sub> films with various particle diameter refer to 175 nm, 230 nm, 280 nm, respectively. They have distinct structural color, blue, green and yellow, respectively.

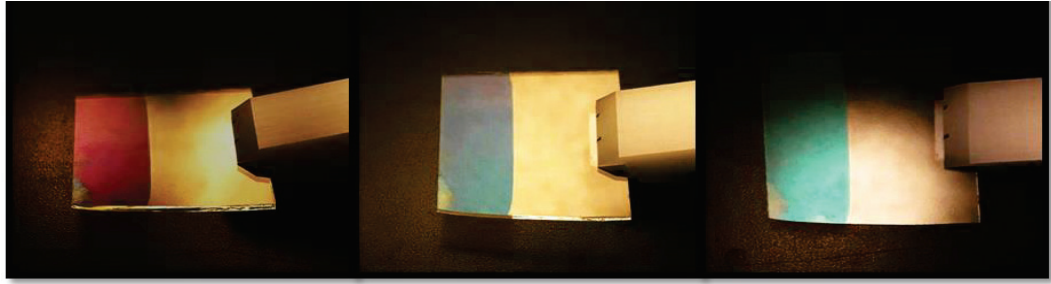


Figure 4.19. Photographs of three-layers SiO<sub>2</sub> films with various angle.

Figure 4.19 shows photographs of the SiO<sub>2</sub> film of three-layer with a diameter of 230 nm. As the incident angle increases, the film's structural color changes from green to violet.

#### 4.7.4. Elastomer P(PEGPEA)/Silica Composite

The composite structure was produced by embedding a non-close packed structure of colloidal SiO<sub>2</sub> particles in an elastomer matrix. First, the photo initiator was dispersed in a PEGPEA monomer. It was subsequently injected into the SiO<sub>2</sub> film produced by the LB method. After waiting for about 30 minutes, the film was subjected to UV light to perform the photopolymerization process. As a result, P(PEGPEA)/SiO<sub>2</sub> composite elastomer composite film was achieved (Figure 3.3) SEM images (Figure 4.20) examined the morphological characteristics of composite films produced with three different sizes of colloidal SiO<sub>2</sub> particles. It is seen that the colloidal assemblies were obtained through the LB method are successfully transferred to the polymer matrix without any deformity. In SEM images, red lines indicate hexagonal domains due to periodic patterns in the structure.

Figure 4.21 presents the cross-section SEM image of elastomer composite with a particle size of 230 nm. The P (PEGPEA) matrix fills in the gaps between the colloidal SiO<sub>2</sub> particles and the composite film of three-layer is obtained. The dwell time before photopolymerization is enough to allow the particles to be integrated into the polymer matrix. The thickness of three-layer of the colloidal SiO<sub>2</sub> particles calculated from the cross-section image of 230 nm particles is about 680 nm. This result indicates that the corresponding SiO<sub>2</sub> layer thickness is approximately three times greater than the colloidal SiO<sub>2</sub> particles size, which means that the three-layer colloidal SiO<sub>2</sub> particles has been successfully transferred to the polymer matrix.

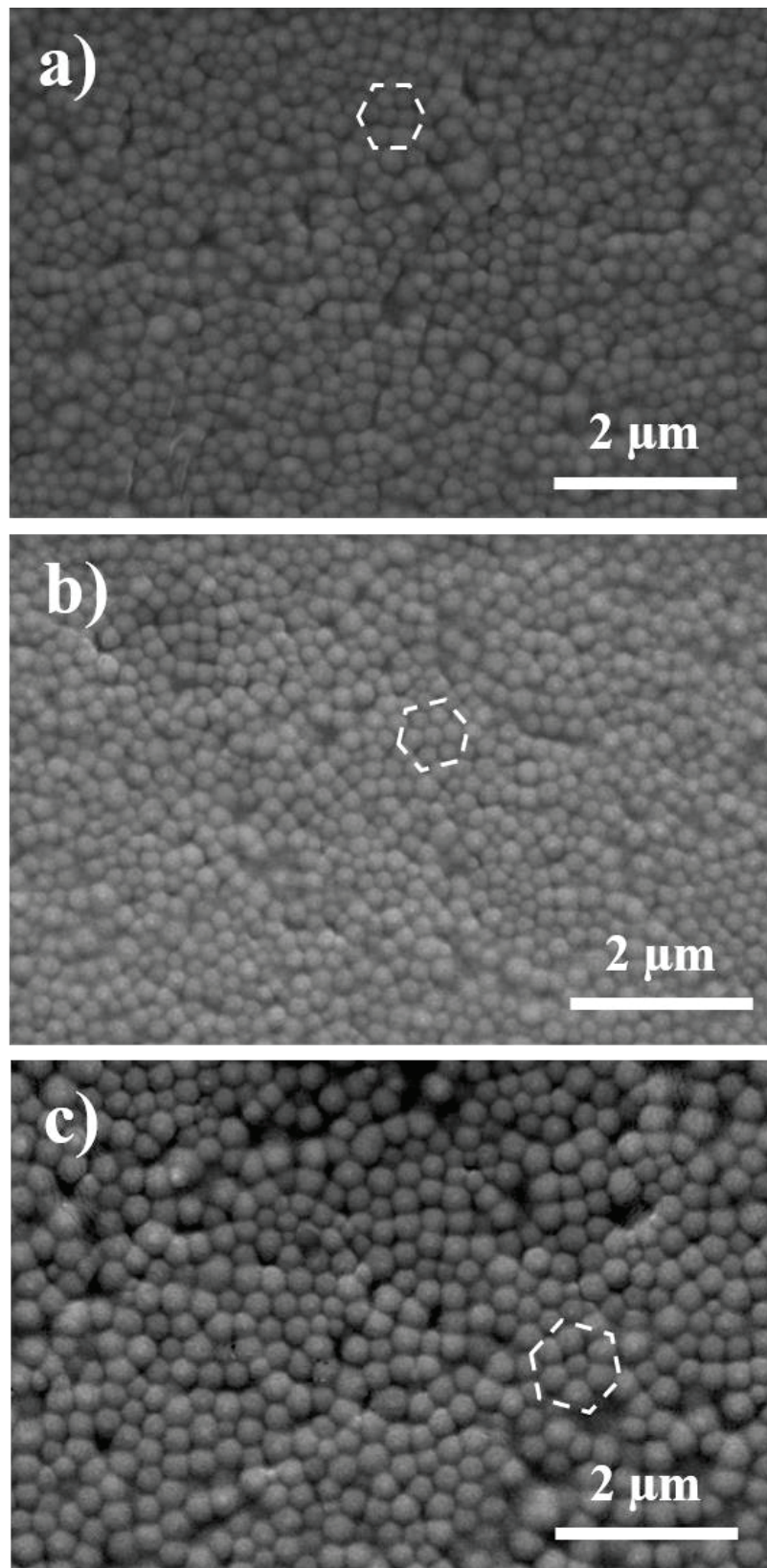


Figure 4.20. SEM images of P(PEGPEA)/ SiO<sub>2</sub> composite film.

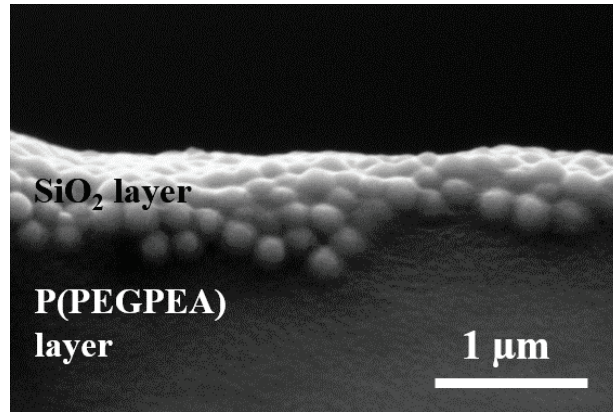


Figure 4.21. SEM cross section images of 230 nm composite film.

The color of the SiO<sub>2</sub>-coated layer distinguished by the naked eye because the uncoated portion of the SiO<sub>2</sub> film P(PEGPEA) is transparent. Distinct structural colors were observed in the elastomer composite film produced, blue and green, respectively (Figure 4.22). The difference in refractive index between SiO<sub>2</sub> ( $n_{silica}$ : 1.45) and P(PEGPEA,  $n_{polymer}$ :1.503) is low. This difference causes the incident light to scatter from the stopband. Accordingly, structural color films are formed.

Normalized reflection spectra of P(PEGPEA)/ SiO<sub>2</sub> composite film is given in Figure 4.23. The signal of reflection wavelength shifts from 554 to 480 nm depending on increasing incident angle. The shifts indicate the existence of periodic structure based on Bragg-Snell law. The difference in wavelength between a bare colloidal array and a polymer array is 64 nm in incident angle of 0°.

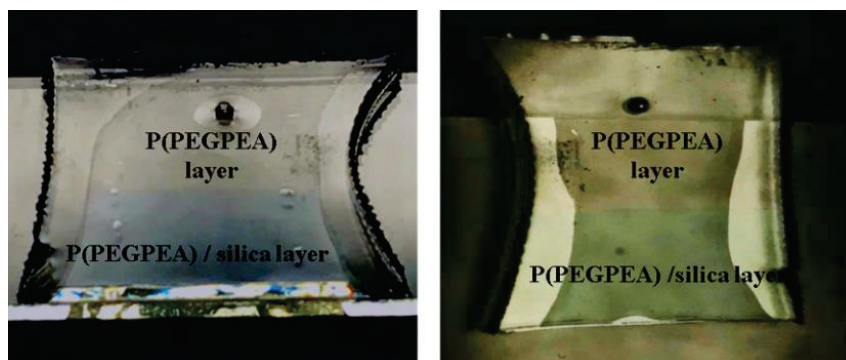


Figure 4.22. Photographs of P(PEGPEA)/SiO<sub>2</sub> composite film with various angles.

The composite structure's elastomer property and its ability to changing color depending on the incident angle make it suitable for use in mechanical sensor applications. For this purpose, the optical properties of the material upon stretching were

investigated. External stimuli are mechanical lateral forces and incident light. The resulting structural color is obtained with the change in the material's structure (changing of interplanar distance) depending on the strain( $\epsilon_x$ ) level. The optical properties of the P(PEGPEA)/SiO<sub>2</sub> film are examined by reflectance values in various strain( $\epsilon_x$ ). The reflectance in various strains ( $\epsilon_x$ ) was presented in Figure 4.24. As the amount of stretching is increased, the reflection signal shifts to lower wavelengths. Due to the reduction in elastomer film thickness, the interplanar distance decreases with the stretching process, which means the spectrum shifts to the blue region (Figure 4.25). The peak position is approximately 496 nm while the strain ( $\epsilon_x$ ) is 0.50.

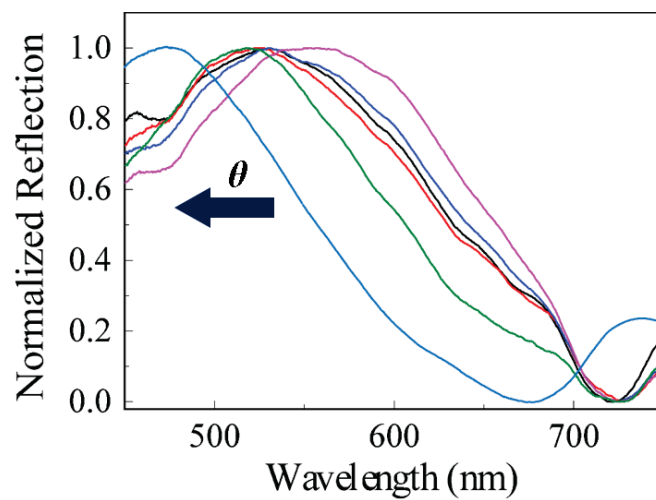


Figure 4.23. Normalized reflection spectra of P(PEGPEA)/SiO<sub>2</sub> composite film.

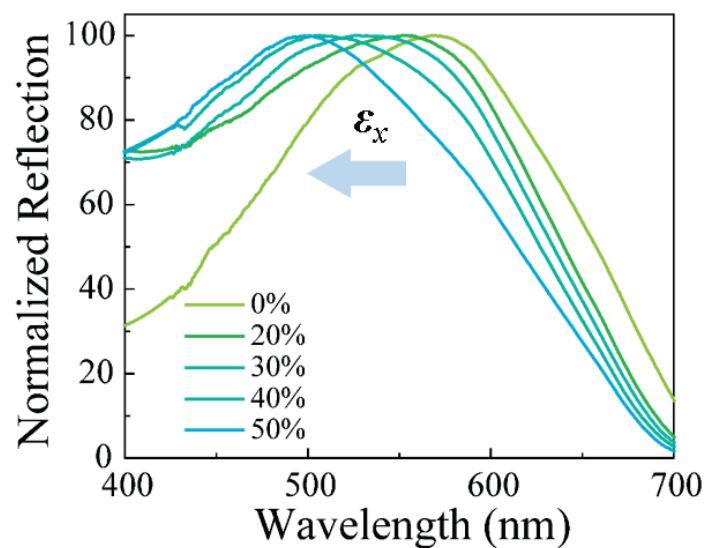


Figure 4.24. Reflection spectra of the P(PEGPEA)/silica composite film upon lateral strain.



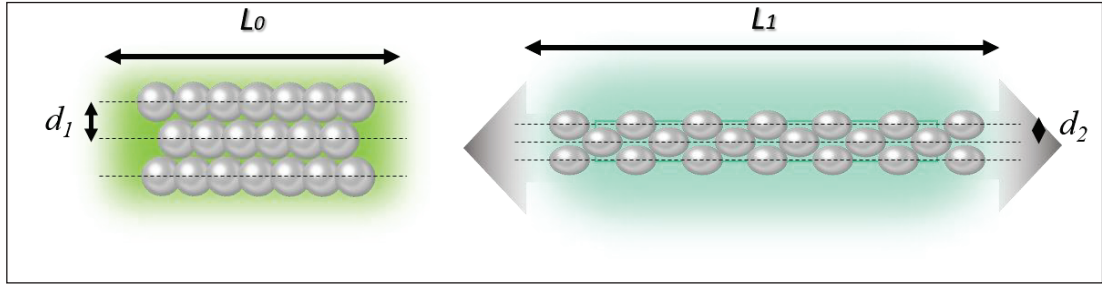


Figure 4.25. Schematic representation of structure of the strain responsive elastomer.

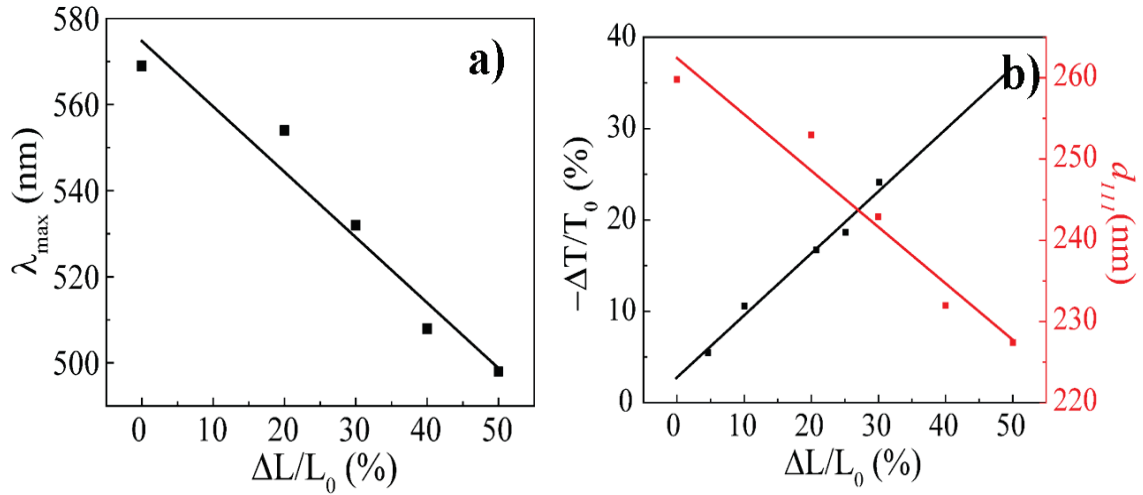


Figure 4.26. Change in (a) reflection signal, (b) thickness, and  $d$  (111) as a function of applied strain.

Because the elastomer composite contains only trace amounts of colloidal SiO<sub>2</sub> particles, its mechanical behavior would be comparable to bare and bulk P(PEGPEA). Due to the proportional relationship between interplanar distance and reflection, the change in  $\lambda_{max}$  by stretching may indicate Poisson's ratio. According to (Figure 4.26 (a)), the decreasing regime ( $\frac{\Delta\lambda_{max}}{\Delta\epsilon_x}$ ) can be noticed that 0.73. Also, the change in the film's interplanar distance as well as the film's thickness is specified in Figure 4.26 (b). Unsurprisingly, Poisson's ratio of the film ( $-\frac{\Delta T}{\Delta L}$ ) is found as 0.79, which is close to change in reflection upon stretching.

Figure 4.27 shows strain-induced change in reflection. It can be understood that it is reversible process and optical response is fully recovered by removing the external force. Since the particles are completely embedded in the rubber-like matrix, in three-dimensional space they are unable to modify their location. Therefore, stable particle

position causes to complete residual strain recovery. Further reversibility of the optical properties was examined by stretching-releasing cycles. The reflection peak position remains unchanged even after 40% strained and cycle in three times.

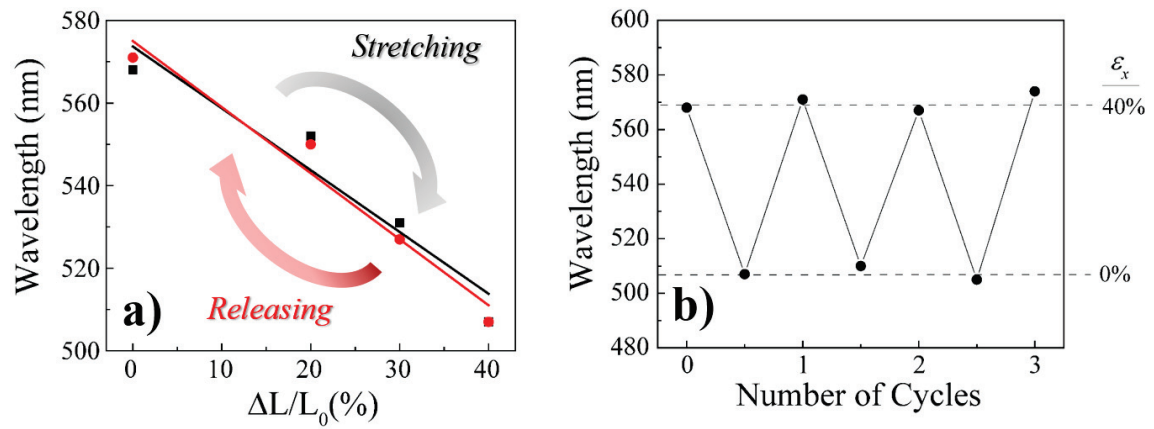


Figure 4.27. Reversible optical properties of the films; (a) alter in reflection upon gradual stretching-releasing. (b) The reflection signals as a function of cycles between lateral strains of 0-40%.

## CHAPTER 5

### CONCLUSIONS

In this thesis, the fabrication of colloidal photonic crystals by using Langmuir Blodgett technique and their integration of polymer matrix was investigated. Firstly, monodispersed colloidal SiO<sub>2</sub> particles were prepared by Stöber Process. Then, three-layer colloidal SiO<sub>2</sub> particles were deposited on the glass substrate. The resulting films show angle-dependent (iridescent) structural color based on coherent scattering from periodic array. The reflection signal shifts from 430 nm to 370 nm, 490 nm to 420 nm, 645 nm to 575 nm while the diameter of the colloidal SiO<sub>2</sub> particles changes from 175 nm, 230 nm, and 280 nm, respectively.

Afterward, they were embedded in elastomeric P(PEGPEA) matrix to create stretchable and colorful composite films by using various fabrication methods including drop-casting and photopolymerization. Iridescent elastomer composite film was achieved by using photopolymerization method. Then, strain responsive properties of P(PEGPEA)/SiO<sub>2</sub> composite films were investigated. As the amount of strain( $\epsilon_x$ ) is increased from the 0% to 50%, the reflection signal shifts from 575 nm to 496 nm due to the reduction in elastomer film thickness and the interplanar distance. Moreover, the reversibility of the produced films was examined by applying stretching-releasing cycles in three times between %0 and %40. As a result, the reflection signal position remains unchanged. This result suggests that there is no hysteresis for these composite materials at least in this limited number of cycles.

In summary, Langmuir Blodgett method provides periodic and controllable layer deposition of SiO<sub>2</sub> colloidal particles. Moreover, elastomer composite structures of these photonic films may be promising candidates for use in the strain sensor applications. Their iridescent colors and strain responsive, and environmentally friendly properties render them robust materials for futuristic applications.

## REFERENCES

1. Kinoshita, S., *Structural colors in the realm of nature*. World Scientific: 2008.
2. Sanders, J., Colour of precious opal. *Nature* **1964**, *204* (4964), 1151.
3. Liu, F.; Dong, B.; Zhao, F.; Hu, X.; Liu, X.; Zi, J., Ultranegetive angular dispersion of diffraction in quasicrystalline biophotonic structures. *Optics express* **2011**, *19* (8), 7750-7755.
4. Zi, J.; Yu, X.; Li, Y.; Hu, X.; Xu, C.; Wang, X.; Liu, X.; Fu, R., Coloration strategies in peacock feathers. *Proceedings of the National Academy of Sciences* **2003**, *100* (22), 12576-12578.
5. Sato, O.; Kubo, S.; Gu, Z.-Z., Structural color films with lotus effects, superhydrophilicity, and tunable stop-bands. *Accounts of Chemical Research* **2008**, *42* (1), 1-10.
6. Zhao, Y.; Xie, Z.; Gu, H.; Zhu, C.; Gu, Z., Bio-inspired variable structural color materials. *Chemical Society Reviews* **2012**, *41* (8), 3297-3317.
7. Aguirre, C. I.; Reguera, E.; Stein, A., Tunable colors in opals and inverse opal photonic crystals. *Advanced Functional Materials* **2010**, *20* (16), 2565-2578.
8. Masuda, Y.; Itoh, T.; Koumoto, K., Self-assembly patterning of silica colloidal crystals. *Langmuir* **2005**, *21* (10), 4478-4481.
9. Jiang, P.; McFarland, M. J., Large-scale fabrication of wafer-size colloidal crystals, macroporous polymers and nanocomposites by spin-coating. *Journal of the American Chemical Society* **2004**, *126* (42), 13778-13786.
10. Zeng, Q.; Ding, C.; Li, Q.; Yuan, W.; Peng, Y.; Hu, J.; Zhang, K.-Q., Rapid fabrication of robust, washable, self-healing superhydrophobic fabrics with non-iridescent structural color by facile spray coating. *RSC Advances* **2017**, *7* (14), 8443-8452.
11. Katagiri, K.; Uemura, K.; Uesugi, R.; Inumaru, K.; Seki, T.; Takeoka, Y., Structurally colored coating films with tunable iridescence fabricated via cathodic electrophoretic deposition of silica particles. *RSC Advances* **2018**, *8* (20), 10776-10784.
12. Kim, M. H.; Im, S. H.; Park, O. O., Rapid Fabrication of Two-and Three-Dimensional Colloidal Crystal Films Via Confined Convective Assembly. *Advanced functional materials* **2005**, *15* (8), 1329-1335.

13. Topçu, G.; Güner, T.; Demir, M. M., Non-iridescent structural colors from uniform-sized SiO<sub>2</sub> colloids. *Photonics and Nanostructures-Fundamentals and Applications* **2018**, *29*, 22-29.
14. Viel, B.; Ruhl, T.; Hellmann, G. P., Reversible deformation of opal elastomers. *Chemistry of Materials* **2007**, *19* (23), 5673-5679.
15. Ge, D.; Lee, E.; Yang, L.; Cho, Y.; Li, M.; Gianola, D. S.; Yang, S., A Robust Smart Window: Reversibly Switching from High Transparency to Angle-Independent Structural Color Display. *Advanced Materials* **2015**, *27* (15), 2489-2495.
16. Ni, Y.; Puthenkovilakom, R. R.; Huo, Q., Synthesis and Supramolecular Self-Assembly Study of a Novel Porphyrin Molecule in Langmuir and Langmuir–Blodgett Films. *Langmuir* **2004**, *20* (7), 2765-2771.
17. Erdogan, M.; Özbek, Z.; Çapan, R.; Yagci, Y., Characterization of polymeric LB thin films for sensor applications. *Journal of Applied Polymer Science* **2012**, *123* (4), 2414-2422.
18. Guo, Y.; Tang, D.; Du, Y.; Liu, B., Controlled fabrication of hexagonally close-packed Langmuir–Blodgett silica particulate monolayers from binary surfactant and solvent systems. *Langmuir* **2013**, *29* (9), 2849-2858.
19. Sun, J.; Bhushan, B.; Tong, J., Structural coloration in nature. *Rsc Advances* **2013**, *3* (35), 14862-14889.
20. Parker, A. R., 515 million years of structural colour. *Journal of Optics A: Pure and Applied Optics* **2000**, *2* (6), R15.
21. Hooke, R., *Micrographia: or some physiological descriptions of minute bodies made by magnifying glasses, with observations and inquiries thereupon*. Courier Corporation: **2003**.
22. Rayleigh, L., VII. On the optical character of some brilliant animal colours. *The London, Edinburgh, and Dublin Philosophical Magazine and Journal of Science* **1919**, *37* (217), 98-111.
23. Merritt, E., A Spectrophotometric Study of Certain Cases of Structural Color I. *JOSA* **1925**, *11* (2), 93-98.
24. Mason, C. W., Structural colors in insects. I. *The Journal of Physical Chemistry* **1926**, *30* (3), 383-395.
25. Mason, C. W., Structural colors in insects. II. *The Journal of Physical Chemistry* **1927**, *31* (3), 321-354.
26. Kinoshita, S.; Yoshioka, S.; Miyazaki, J., Physics of structural colors. *Reports on Progress in Physics* **2008**, *71* (7), 076401.

27. Zhang, J.-Z.; Gu, Z.-Z.; Chen, H.-H.; Fujishima, A.; Sato, O., Inverse mopho butterfly: A new approach to photonic crystal. *Journal of nanoscience and nanotechnology* **2006**, *6* (4), 1173-1176.
28. Kinoshita, S.; Yoshioka, S., Structural colors in nature: the role of regularity and irregularity in the structure. *ChemPhysChem* **2005**, *6* (8), 1442-1459.
29. Greenewalt, C. H.; Brandt, W.; Friel, D. D., Iridescent colors of hummingbird feathers. *JOSA* **1960**, *50* (10), 1005-1013.
30. Vigneron, J. P.; Simonis, P., Natural photonic crystals. *Physica B: Condensed Matter* **2012**, *407* (20), 4032-4036.
31. Joannopoulos, J. D.; Johnson, S. G.; Winn, J. N.; Meade, R. D., Molding the flow of light. *Princeton Univ. Press, Princeton, NJ [ua]* **2008**.
32. Armstrong, E.; O'Dwyer, C., Artificial opal photonic crystals and inverse opal structures—fundamentals and applications from optics to energy storage. *Journal of Materials Chemistry C* **2015**, *3* (24), 6109-6143.
33. Phillips, K. R.; England, G. T.; Sunny, S.; Shirman, E.; Shirman, T.; Vogel, N.; Aizenberg, J., A colloidoscope of colloid-based porous materials and their uses. *Chemical Society Reviews* **2016**, *45* (2), 281-322.
34. Tilley, R. J., *Colour and the optical properties of materials: an exploration of the relationship between light, the optical properties of materials and colour*. John Wiley & Sons: 2010.
35. Whitesides, G. M.; Grzybowski, B., Self-assembly at all scales. *Science* **2002**, *295* (5564), 2418-2421.
36. Robb, M. J.; Ku, S. Y.; Hawker, C. J., 25th Anniversary article: No assembly required: Recent advances in fully conjugated block copolymers. *Advanced Materials* **2013**, *25* (40), 5686-5700.
37. Josephson, D. P.; Miller, M.; Stein, A., Inverse Opal SiO<sub>2</sub> Photonic Crystals as Structurally-Colored Pigments with Additive Primary Colors. *Zeitschrift für anorganische und allgemeine Chemie* **2014**, *640* (3-4), 655-662.
38. Shiu, J.-Y.; Kuo, C.-W.; Chen, P.; Mou, C.-Y., Fabrication of tunable superhydrophobic surfaces by nanosphere lithography. *Chemistry of materials* **2004**, *16* (4), 561-564.
39. Schäfer, C. G.; Smolin, D. A.; Hellmann, G. P.; Gallei, M., Fully reversible shape transition of soft spheres in elastomeric polymer opal films. *Langmuir* **2013**, *29* (36), 11275-11283.
40. Zhou, M.; Bao, J.; Xu, Y.; Zhang, J.; Xie, J.; Guan, M.; Wang, C.; Wen, L.; Lei, Y.; Xie, Y., Photoelectrodes based upon Mo: BiVO<sub>4</sub> inverse opals for photoelectrochemical water splitting. *Acs Nano* **2014**, *8* (7), 7088-7098.

41. Pikul, J. H.; Zhang, H. G.; Cho, J.; Braun, P. V.; King, W. P., High-power lithium ion microbatteries from interdigitated three-dimensional bicontinuous nanoporous electrodes. *Nature communications* **2013**, *4*, 1732.
42. Ito, T.; Katsura, C.; Sugimoto, H.; Nakanishi, E.; Inomata, K., Strain-responsive structural colored elastomers by fixing colloidal crystal assembly. *Langmuir* **2013**, *29* (45), 13951-13957.
43. Rajca, A., An Introduction To Ultrathin Organic Films: From Langmuirblodgett To Self-Assembly, By Abraham Ulman, Academic Press, London 1991, Xxiii, 442Pp., \$65, ISBN 0-12-708230-1. *Advanced Materials* **1992**, *4* (4), 309-309.
44. Devaux, H., Dünne Lamellen und ihre physikalischen Eigenschaften. *Kolloid-Zeitschrift* **1932**, *58* (3), 260-276.
45. Oliveira Jr, O. N., Langmuir-Blodgett films-properties and possible applications. *Braz J Phys* **1992**, *22* (2), 60-69.
46. Petty, M. C., *Langmuir-Blodgett films: an introduction*. Cambridge University Press: 1996.
47. Acharya, S.; Bhattacharjee, D.; Sarkar, J.; Talapatra, G., Spectroscopic study of non-amphiphilic 2-(4-biphenyl)-5-(4-tert-butylphenyl)-1,3,4-oxadiazole aggregates at air–water interface and in Langmuir–Blodgett films. *Chemical physics letters* **2004**, *393* (1-3), 1-6.
48. Ferreira, M.; Dinelli, L. s. R.; Wohnrath, K.; Batista, A. A.; Oliveira Jr, O. N., Langmuir–Blodgett films from polyaniline/ruthenium complexes as modified electrodes for detection of dopamine. *Thin Solid Films* **2004**, *446* (2), 301-306.
49. Kaganer, V. M.; Möhwald, H.; Dutta, P., Structure and phase transitions in Langmuir monolayers. *Reviews of Modern Physics* **1999**, *71* (3), 779.
50. Vivero-Escoto, J. L.; Slowing, I. I.; Trewyn, B. G.; Lin, V. S. Y., Mesoporous silica nanoparticles for intracellular controlled drug delivery. *Small* **2010**, *6* (18), 1952-1967.
51. Carcouët, C. C.; Van De Put, M. W.; Mezari, B.; Magusin, P. C.; Laven, J.; Bomans, P. H.; Friedrich, H.; Esteves, A. C. C.; Sommerdijk, N. A.; Van Benthem, R. A., Nucleation and growth of monodisperse silica nanoparticles. *Nano letters* **2014**, *14* (3), 1433-1438.
52. Szekeres, M.; Kamalin, O.; Schoonheydt, R. A.; Wostyn, K.; Clays, K.; Persoons, A.; Dékány, I., Ordering and optical properties of monolayers and multilayers of silica spheres deposited by the Langmuir–Blodgett method. *Journal of Materials Chemistry* **2002**, *12* (11), 3268-3274.

53. Romanov, S. G.; Orlov, S.; Ploss, D.; Weiss, C. K.; Vogel, N.; Peschel, U., Engineered disorder and light propagation in a planar photonic glass. *Scientific reports* **2016**, *6*, 27264.
54. Comoretto, D.; Grassi, R.; Marabelli, F.; Andreani, L., Growth and optical studies of opal films as three-dimensional photonic crystals. *Materials Science and Engineering: C* **2003**, *23* (1-2), 61-65.